Chemical Engineering Report Series
Kemian laitetekniikan raporttisarja No. 54
Espoo 2009

MODELLING GAS-LIQUID FLOW IN TRICKLE-BED REACTORS

Katja Lappalainen

TEKNILLINEN KORKEAKOULU
TEKNISKA HÖGSKOLAN
HELSINKI UNIVERSITY OF TECHNOLOGY
TECHNISCHE UNIVERSITÄT HELSINKI
UNIVERSITE DE TECHNOLOGIE D'HELSINKI

Chemical Engineering Report Series
Kemian laitetekniikan raporttisarja No. 54
Espoo 2009

MODELLING GAS-LIQUID FLOW IN TRICLE-BED REACTORS

Katja Lappalainen

Dissertation for the degree of Doctor of Science in Technology to be presented with due permission for public examination and debate in Auditorium V1 at Helsinki University of Technology (Espoo, Finland) on the 5th of June, 2009, at 12 noon.

Helsinki University of Technology
Department of Biotechnology and Chemical Technology
Chemical Engineering

Teknillinen korkeakoulu
Biotekniikan ja kemian tekniikan laitos
Kemian laitetekniikka

Distribution:
Helsinki University of Technology
Department of Biotechnology and Chemical Technology
P. O. Box 6100
FIN-02015 TKK
Tel. + 358-9-451 2634
Fax. +358-9-451 2694
E-mail: katja.lappalainen@iki.fi

ISBN 978-951-22-9885-3
ISSN 1236-875X

Multiprint Oy
Espoo 2009

ABSTRACT

The performance of a trickle-bed reactor is affected, not only by reaction kinetics, pressure, and temperature, but also by reactor hydrodynamics, which are commonly described by means of global parameters such as pressure drop, liquid holdup, dispersion of gas and liquid phases, catalyst wetting, and mass- and heat-transfer coefficients. Due to the complicated nature of trickle-bed reactor hydrodynamics, there is no straightforward method for the scale-up of these parameters from laboratory to industrial scale. Scale-up has therefore been based on a combination of different procedures: 1) constant dimensionless groups, 2) mathematical modeling, and 3) pilot planting. In general, not all dimensionless groups can be kept constant and pilot planting is both time-consuming and expensive. Thus mathematical modeling is an interesting option for the design of new trickle-bed reactors. In addition, mathematical models can be used in performance and sensitivity analysis. In this work mathematical models have been developed for pressure drop, liquid holdup, dispersion, and catalyst wetting efficiency and different modeling options are also discussed.

Global pressure drop and liquid holdup can be estimated from the gas-liquid-solid phase interaction models by formulating a simplified mass and momentum equation for gas and liquid phase. New improved phase interaction models have been developed assuming uniformly distributed gas and liquid flows. Although it is assumed that the liquid is distributed uniformly, the perfect wetting of the catalyst is not assumed. A new model for liquid-solid wetting efficiency has been developed concurrently with the phase interaction models. The liquid-solid wetting efficiency is used to determine the significance of gas-liquid, liquid-solid and gas-solid phase interactions. Phase interaction and wetting efficiency model parameters have been optimized against a large experimental database for pressure drop, liquid holdup, and wetting efficiency.

CFD is used to model phase dispersion in non-uniform gas and liquid flow conditions, where plug flow cannot be assumed. Spreading is attributed to three separate factors: overloading, mechanical dispersion, and capillary dispersion. The first of the spreading mechanisms derives from the phase interactions and does not require a separate model. New models have been developed for mechanical and capillary dispersion. The performance of the dispersion models is discussed on the basis of multiple case studies. The ability of the hydrodynamic model developed here is compared to liquid dispersion experiments from four different literature sources, including the author's own experiments.

In addition to CFD modeling, an alternative, potential tool for liquid distribution studies is also presented – the cellular automata model. Thanks to single event modeling, a cellular automata model is simpler and thus faster and would be better suited for the modeling of larger reactors, when information on pressure drop and liquid holdup is not required.

TIIVISTELMÄ

Triklekerrosreaktorin toimintaan vaikuttaa reaktorikinetiikan, paineen ja lämpötilan lisäksi myös reaktorin hydrodynamiikka. Tavallisesti hydrodynamiikkaa kuvataan globaalien parametrien avulla: painehäviö, reaktorin nestesisältö (holdup), kaasun ja nesteen leviäminen (dispersio), katalyytin kastuminen sekä massan- ja lämmönsiirtokertoimet. Koska hydrodynamiikalla on merkittävä vaikutus triklekerrosreaktoreiden toimintaan, edellä mainitut parametrit pyritään pitämään vakiona reaktorin kokoa kasvatettaessa. Tähän ei kuitenkaan ole olemassa suoraviivaista menetelmää hydrodynamiikan monimutkaisuuden vuoksi. Triklekerrosreaktoreiden mittakaavan muunnos (scale-up) tehdäänkin tavallisesti eri menetelmien yhdistelmänä, joita ovat 1) dimensiottomien ryhmien pitäminen vakiona, 2) matemaattinen mallinnus ja 3) tutkimus eri kokoluokan koelaitteistoilla (pilot planting). Kaikkien dimensiottomien ryhmien pitäminen vakiona samanaikaisesti ei ole kuitenkaan yleensä mahdollista ja tutkimus eri kokoluokan koelaitteistoilla on sekä aikaa vievää että kallista, minkä vuoksi matemaattinen mallinnus on kiinnostava vaihtoehto uusien triklekerrosreaktoreiden suunnittelutyökaluna. Matemaattisten mallien käyttö ei myöskään rajoitu uusien reaktoreiden suunnitteluun, vaan mallinnusta voidaan käyttää myös suorituskyky- ja herkkyysanalyyseihin. Tässä väitöskirjassa on kehitetty matemaattiset mallit painehäviölle, reaktorin nestesisällölle, dispersiolle sekä katalyytin kastumisen tehokkuudelle (wetting efficiency). Lisäksi työssä on keskusteltu eri mallinnusvaihtoehdoista.

Triklekerrosreaktorin painehäviölle ja nestesisällölle voidaan laskea arvio kaasu-neste-kiinteä vuorovaikutusvoimien perusteella muodostamalla ensin yksinkertaistetut massa- ja liikemääräyhtälöt kaasulle ja nesteelle. Kehitettäessä malleja kaasu-neste-kiinteä vuorovaikutusvoimille on oletettu, että kaasu ja neste ovat tasaisesti jakautuneet reaktorin poikkipinta-alalle, mutta katalyytti ei välttämättä ole täydellisesti kastunut. Uusi malli katalyytin kastumisen tehokkuudelle kehitettiin samanaikaisesti vuorovaikutusvoimien kanssa. Katalyytin kastumisen tehokkuus määrittelee kaasu-neste, neste-kiinteä ja kaasu-kiinteä vuorovaikutuksien suhteellisen osuuden. Mallien parametrit on optimoitu laajan mittaustietokannan perusteella, joka sisälsi mittaustuloksia painehäviöstä, nestesisällöstä ja katalyytin kastumisosuudesta, useista eri kirjallisuuslähteistä.

Faasien leviämistä, kun kaasu- ja nestevirtaukset ovat epätasaisesti jakautuneet, mallinnettiin Fluent-virtauslaskentaohjelmistolla. Faasien leviämisen katsottiin aiheutuvan kolmen eri mekanismin vaikutuksesta: liikakuormitus (overloading), mekaaninen dispersio ja kapillaaridispersio. Liikakuormitus aiheutuu kaasu-neste-kiinteä vuorovaikutusvoimista eikä tarvitse erillistä dispersiomallia. Uudet dispersiomallit kehitettiin mekaaniselle ja kapillaaridispersiolle. Dispersiomallien toimintaa arvioitiin useiden simulointitapausten perusteella – mallin ennustamaa nesteenjakautumista verrattiin mittauksiin neljästä eri kirjallisuuslähteestä, mukaan lukien omat mittaukset.

Virtauslaskentaohjelmistojen käytön lisäksi esiteltiin myös toinen potentiaalinen työkalu nesteen jakautumisen tutkimiseen – soluautomaattimalli (cellular automata model). Mallin rakenne on perinteisiä virtauslaskentaohjelmistoja yksinkertaisempi ja nopeampi. Se soveltuisi näin ollen paremmin suurempien reaktoreiden nesteenjakautumisen tutkimiseen, kun tieto painehäviöstä ja nestesisällöstä ei ole tarpeellista.

PREFACE

I wrote this thesis during the years 2003-2009 in Helsinki University of Technology in the laboratory of Chemical Engineering and Plant Design, which is today a part of the Department of Biotechnology and Chemical Technology. It was a long project that at times felt as a struggle and at times filled up my mind with excitement. But all along it was a challenge that would have not been possible without the support, wisdom, and guidance of all the people who have more or less directly contributed to this work – even if it was just to lift up my spirit whenever I felt overwhelmed with the project. Nonetheless, despite the hard work, it has been a journey worth traveling!

I began my graduate studies as a continuation of my Master's thesis due to the encouragement from Professor Juhani Aittamaa, who was also the supervisor of this thesis for the first three years. I wish to express my deepest gratitude for giving me the opportunity to start this thesis and for the encouragement and guidance he offered me. I would also thank him for allowing me to work quite independently and freely.

I would also like to thank my current supervisor, professor Ville Alopaeus, and my instructor Mikko Manninen for their guidance and constructive criticism. They have both been working with me from the beginning and their input has been invaluable during the preparation of the papers, improving the models and in overcoming many difficult theoretical problems. They have helped me to make this thesis a reality.

I would like to acknowledge all of the co-authors for their significant contributions to this thesis. A special thank goes to Kristiina Piiri, Suvi Jussila, and Heli Nikiforow for providing me with very insightful laboratory experiments, which opened my mind for all the phenomena occurring in trickle-beds, and for my co-workers who made working in the laboratory quite fun from time to time. Finally I would like to thank Tekes and the industrial partners for financing ModCher-project and its continuation project Regal, during which this thesis was written.

Also my family deserves special thanks. Even though they did not contribute to the scientific part of my thesis, without their support and encouragement the task would have been at least twice as difficult. The last couple of years, working in Espoo and living in Imatra, have been a challenge as regards to time management. I would like to thank my parents for helping me out in any ways they could in that matter. And especially I would like to thank my husband Kai for the support he has offered me, although finishing this thesis has meant constant traveling and absence from home.

Imatra, May 2009

Katja Lappalainen

LIST OF PUBLICATIONS

This thesis is based on the following publications (Appendices I – VI), which are referred to in the text by their Roman numerals:

[I] Alopaeus, V., Hynynen[i], K., Aittamaa, J., 2006. A cellular automata model for liquid distribution in trickle bed reactors, Chemical Engineering Science, 61, 4930−4943.

[II] Alopaeus, V., Hynynen[i], K., Aittamaa, J., Manninen, M., 2006. Modeling of gas-liquid packed-bed reactors with momentum equations and local interaction closures, Industrial & Engineering Chemistry Research, 45, 8189−8198.

[III] Lappalainen, K., Alopaeus, V., Manninen, M., Aittamaa, J., 2008. Improved hydrodynamic model for wetting efficiency, pressure drop, and liquid holdup in trickle-bed reactors, Industrial & Engineering Chemistry Research, 47, 8436–8444.

[IV] Lappalainen, K., Manninen, M., Alopaeus, V., Aittamaa, J., Dodds, J., 2009. An analytical model for capillary pressure − saturation relation for gas-liquid system in a packed-bed of spherical particles, Transport in Porous Media, 77, 17–40.

[V] Lappalainen, K., Manninen, M., Alopaeus, V., 2009. CFD modeling of radial spreading of flow in trickle-bed reactors due to mechanical and capillary dispersion, Chemical Engineering Science, 64, 207–218.

[VI] Lappalainen, K., Alopaeus, V., Manninen, M., Kallio, S., 2008. Modelling of liquid dispersion in trickle-bed reactors: capillary pressure gradients and mechanical dispersion, 11th International Conference on Multiphase Flow in Industrial Plants, September, Palermo, Italy. [ii]

[i] Katja Lappalainen's maiden name was Katja Hynynen
[ii] The conference publication was peer reviewed

AUTHOR'S CONTRIBUTIONS TO THE APPENDED PUBLICATIONS

[I] The author participated in the model development.

[II] The author participated in the model development and result analysis.

[III] The author participated in the model development, optimized the model parameters against literature data, analyzed the results with the co-authors, and wrote the paper.

[IV] The author participated in the model development, performed the testing and validation of the model against literature data, and wrote the paper.

[V] The author participated in the model development and in the implementation of the model to CFD. The author performed the CFD simulations and wrote the paper. The author analyzed the results with the co-authors.

[VI] The author participated in the design and development of the experimental setup and supervised the experiments. The author performed the CFD simulations and wrote the paper. The author analyzed the results with the co-authors.

TABLE OF CONTENTS

1. INTRODUCTION

Trickle-bed reactors are three-phase reactors where gas and liquid flow either concurrently or countercurrently through a packed bed of catalyst, with the liquid flowing downwards. In this thesis the focus is on the concurrent mode of operation. Examples of large industrial applications are, for example, the hydrodesulfurization and catalytic hydrodenitrification of crude oil fractions in oil refining, the oxidative treatment of wastewater, and the historically important synthesis of 2-butyne-1,4-diol from acetylene and formaldehyde (Westerterp and Wammes 2005).

The performance of a trickle-bed reactor is not solely determined by the reaction kinetics and chosen operation pressure and temperature. In addition, reactor hydrodynamics have a strong influence on conversion, yield, and selectivity. Hydrodynamics can be described by means of global hydrodynamic parameters, such as pressure drop, liquid holdup, dispersion of fluid phases, liquid-solid wetting efficiency, flow regime, and mass and heat-transfer coefficients.

In the course of the current work, the performance of the current hydrodynamic models has been analyzed. As a consequence, it has been suggested that in more complicated flow situations, where uniform liquid distribution cannot be assumed, gas-liquid-solid phase interaction models alone do not describe the reactor hydrodynamics sufficiently well. Models for liquid dispersion are required in addition. A liquid point feed may be mentioned as a simple example of non-uniform liquid flow. The development and validation of these phase interaction and dispersion models constitute the core of this dissertation. An outline of the work done within this thesis is summarized below:

- Observation of the liquid flow behavior in an experimental setup, which initiated the development of the cellular automata model for liquid distribution in trickle-bed reactors [I]
- A thorough analysis of hydrodynamic models for trickle-bed reactors in literature is performed. As a result, new phase interaction models based on local hydrodynamics are developed, which includes a novel concept of phase-specific tortuosities and a new liquid-solid wetting efficiency model [II], [III].
- The phase interaction models alone are insufficient for describing liquid spreading in more complicated flow situations, such as liquid point source feed. Liquid spreading is attributed to three mechanisms: overloading, capillary dispersion, and mechanical dispersion. This initiated the development of micro-scale dispersion models for CFD simulations and the validation of these models against literature and the author's own experimental data [IV], [V], [VI].

2. BACKGROUND

2.1 Phase interactions

A model for the two-phase pressure drop and liquid holdup in trickle-bed reactors was developed in papers [II] and [III]. Earlier models included various empirical and phenomenological/semi-empirical models (Table 1). Although the models have been improved over the last few decades, there is still need for further improvements due to the complex nature of the three-phase flow. The basic approach behind all phenomenological hydrodynamic models is similar – separate models are constructed for the gas-liquid-solid phase interactions and those models are then included in the momentum equations of gas and liquid.

Table 1. Hydrodynamics models for trickle-bed reactors.

Approach	Authors	Model basis	Additional remarks
Empirical models for liquid holdup and/or pressure drop			
	Specchia and Baldi (1977) Rao et al. (1983) Larachi et al. (1991) Wammes et al. (1991) Wammes and Westerterp (1991) Pinna et al. (2001)		Pressure drop and liquid holdup
	Tosun (1984) Sai and Varma (1987) Ellman et al. (1988) Ratnam et al. (1993)		Pressure drop
	Sai and Varma (1988) Ellman et al. (1990) Burghardt et al. (1995) Fu and Tan (1996) Bensetiti et al. (1997)* Xiao et al. (2000)		Liquid holdup
Phenomenological models			
	Sáez and Carbonell (1985)	Relative permeability	Gas-liquid interaction force is not included
	Tung and Dhir (1988), Benkrid et al. (1997) Attou et al. (1999), Narasimhan et al. (2002)	Gas and liquid phase force balance	Models are derived based on the gas and liquid phase force balances Apart from Benkrid et al. (1997). models include a twofold consideration of gas-liquid and gas-solid interactions In Benkrid et al. (1997) a separate liquid holdup model is required in high interaction regime
	Fourar et al. (2001)	F-function	The superficial fluid velocity of each fluid is multiplied by a phase-specific F-function that depends on fluid saturation Gas-solid and gas-liquid interactions are not separated, making the model suitable only for uniform flow situations
	Holub et al. (1992, 1993), Al-Dahhan and Duduković (1994) Al-Dahhan et al. (1998), Iliuta and Larachi (1999, 2005) Iliuta et al. (2000a, 2000b)	Slit approach	Local flow is modeled inside a simpler rectangular slit, instead of more complicated averaged equations of motion More sophisticated versions also predict the wetting efficiency

* Neural network correlation

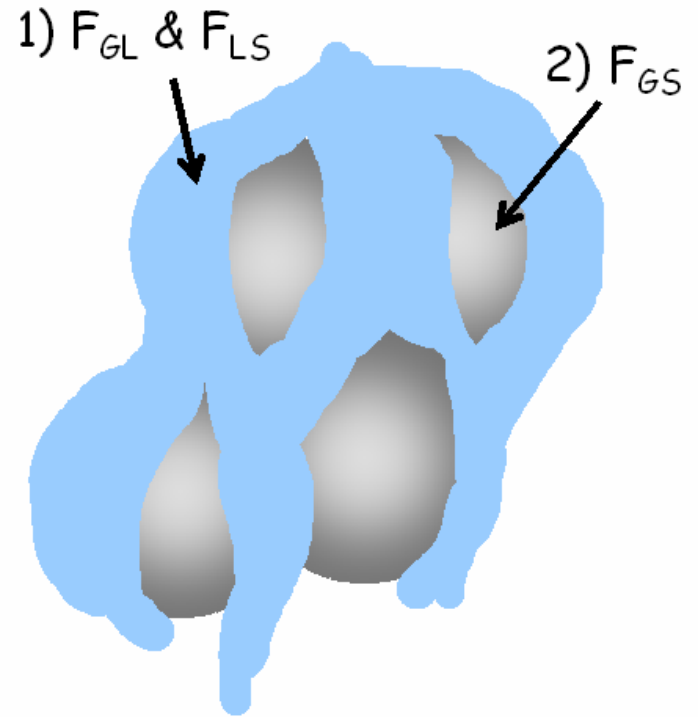

Figure 1. Phase interactions in gas-liquid flow through a packed bed. 1) The particles are covered with a flowing liquid film – the phase interactions present are the gas-liquid and the liquid-solid. 2) Particles are dry or merely covered with a stagnant liquid film – only the gas-solid interaction force is present.

Here the phase interactions are included on the basis of the wetting efficiency of the catalyst, as presented in Figure 1. The wetting efficiency is here defined as the fraction of the catalyst covered with a flowing liquid film. In the wetted parts of the catalyst, the gas-liquid and liquid-solid interactions are present. In the non-wetted parts of the catalyst, only the gas-solid phase interaction is present. A similar approach has also been suggested by Iliuta and Larachi (2005). If the catalyst is partially wetted, the phase interactions are included in proportion as presented in equations (4) and (5).

2.2 Wetting efficiency

A wetting efficiency model was developed in paper [III], simultaneously with the phase interaction models. Wetting efficiency describes the fraction of the catalyst covered with a flowing liquid film. It is used to calculate the total interaction forces from the gas-liquid-solid phase interaction forces, see equations (4) and (5). Literature models for wetting efficiency are presented in Table 2. The majority of the literature models are developed based on a relatively small wetting efficiency database and only in the slit-models has the wetting efficiency model been developed simultaneously with the gas-liquid-solid phase interaction models.

Table 2. Literature correlations for the wetting efficiency, f_e.

Source	Correlation
Al-Dahhan and Duduković (1995) • *Tracer method* • *High pressure* • *No external data*	$f_e = 1.104\left(\mathrm{Re}'_L\right)^{1/3}\left[\dfrac{1+\left[\left(\Delta P/\Delta L\right)/\rho_L g\right]}{\mathrm{Ga}'_L}\right]^{1/9}$
Alicilar et al. (1994) • *Tracer method* • *No external data*	$f_e = 1-\dfrac{25.353}{\mathrm{Re}_L^{0.96}}$ $180 > \mathrm{Re}_L > 35$
Burghardt et al. (1995) • *Tracer method* • *Only one gas-liquid system, generalization based on an analogy with typical correlation for wetting efficiency* • *No external data*	$f_e = 3.38\,\mathrm{Re}_L^{0.222}\,\mathrm{Re}_G^{-0.083}\left(d_p\sqrt[3]{\dfrac{g\rho_L^2}{\mu_L^2}}\right)^{-0.512}$
El-Hisnawi et al. (1982) • *Tracer method*	$f_e = 1.617\,\mathrm{Re}_L^{0.146}\mathrm{Ga}_L^{-0.071}$ $f_e = 1.02 S_{L,dyn}^{0.244}$
González-Mendizabal et al. (1998) • *Reaction rate method*	$f_e = 1-\exp\left[-4.265\cdot 10^{-2}\left(\mathrm{Re}'_L\right)^{0.745}\left(\mathrm{Re}'_G\right)^{0.079}\right]$ $6.71 < \mathrm{Re}'_L < 117.90 \quad 32.00 < \mathrm{Re}'_G < 204.19$
Herskowitz (1981) • *Reaction rate method* • *Measurements in Herskowitz et al. (1979)*	$f_e = 1.301 + 0.0739\ln\dfrac{U_L}{m/s}$ $0.0002 < U_L < 0.01\ m/s$
Herskowitz and Smith (1983) • *The background of the correlation was not reported*	$f_e = 0.77\left(\dfrac{L_m}{kg/ms^2}\right)^{0.1}$
Kundu et al. (2003) • *Based on the model presented in Pironti et al. (1999)* • *Model performance is strongly affected by the performance of the two-phase hydrodynamic model and by the Ergun parameters*	$f_e = \dfrac{2F_I + \left(F_{PG}\right)_{G-\mathrm{filled}} + \varepsilon\{\rho_L g\tau - dp/dz\} - \theta_G\{g\tau - 2dp/dz\}}{\left(F_{PL}\right)_{L-\mathrm{filled}} - \left(F_{PG}\right)_{G-\mathrm{filled}}}$ $\{(-dp/dz)_{L-\mathrm{filled}} + \rho_L g\tau\}\varepsilon = \left(F_{PL}\right)_{L-\mathrm{filled}}$ $\{(-dp/dz)_{G-\mathrm{filled}} + \rho_G g\tau\}\alpha = \left(F_{PG}\right)_{G-\mathrm{filled}}$ $\{(-dp/dz) + \rho_L g\tau\}(1-\alpha)\varepsilon = F_{PL} - F_I$ The particle-fluid interaction forces, F_{Pk}, the liquid-gas interfacial drag F_I and the tortuosity, τ, are calculated based on Narasimhan et al. (2002) The Ergun equation is used for the one-phase pressure drop

Table 2 (continued)

Source	Correlation
Larachi et al. (2001) • *Neural network correlation*	$f_e = 0.83S^* + 0.17$ $1/S^* = 1 + \exp\left[-\sum_{j=1}^{8} \omega_j H_j\right]$ $1/H_j = 1 + \exp\left[-\sum_{i=1}^{6} \omega_{ij} U_i^*\right]$ The normalized input groups (U_i^*) and connectivity weights (ω) are presented in Table 3 of the corresponding reference
Mills and Duduković (1981) • *Tracer method* • *5 parameters were fitted based on only 26 data points* • *No external data*	$f_e = \sqrt{\frac{D_{TP}}{D_{LF}}}$ $= 1.0 - \exp\left[-1.35\,\mathrm{Re}_L^{0.333}\left(\mathrm{Fr}_L^*\right)^{0.235}\left(\mathrm{We}_L^*\right)^{-0.170}\left(\frac{\left(a_t d_p^2\right)/cm}{\varepsilon^2}\right)^{-0.0425}\right]$ $f_e = \sqrt{\frac{D_{TP}}{D_{LF}}}$ $= \tanh\left[0.664\,\mathrm{Re}_L^{0.333}\left(\mathrm{Fr}_L^*\right)^{0.195}\left(\mathrm{We}_L^*\right)^{-0.171}\left(\frac{\left(a_t d_p^2\right)/cm}{\varepsilon^2}\right)^{-0.0615}\right]$
Ring and Missen (1991) • *Tracer method* • *No external data*	$f_e = \sqrt{\frac{D_{TP}}{D_{LF}}} = 1 - \exp\left(-118\left(\frac{U_L}{m/s}\right)^{0.635}\right)$

2.3 Liquid dispersion

In a two-phase flow through a packed bed, dispersion arises from three mechanisms: overloading, capillary dispersion, and mechanical dispersion. The mechanisms are summarized below and the flow parameters affecting each dispersion force are reviewed in Table 3.

- **Overloading** occurs if the local liquid flow exceeds the local capacity of the catalyst bed. If the flow is uniform, an increase in the overall pressure drop is observed, but if the capacity is exceeded only locally, liquid will spread sideways to minimize the pressure drop, and overloading occurs. Overloading appears usually at the top of the bed, right after the liquid distributor (Hoek et al. 1986; Porter et al. 1978). Since overloading is caused by a two-phase pressure drop, it results from the total interaction forces in CFD simulations.
- **Mechanical dispersion** results from the variation of the small-scale velocity profiles in porous structures. Fluctuation of the microscopic streamlines in space with respect to the mean direction of the flow causes the flow to spread both horizontally and longitudinally (Bear 1979). The longitudinal dispersion manifests itself through residence time distributions and the transverse dispersion can be observed as the horizontal spreading of flow.
- **Capillary dispersion** is caused by the differences in the local capillary pressures, i.e. capillary pressure gradients. Capillary dispersion is more

pronounced with low porosities and small particle sizes when the capillary pressure is also higher. However, since capillary pressure increases steeply as liquid saturation approaches zero, it will always obtain high values if the liquid saturation is low enough.

Table 3. Flow parameters affecting the dispersion forces. Inverse – dispersion increases as the parameter decreases; Neutral – the parameter has no effect; Direct – dispersion increases as the parameter increases; Unclassified – the effect has not been researched or is inconclusive.

Dispersion mechanism	Effect			
	Inverse	**Neutral**	**Direct**	**Unclassified**
Overloading	Particle size Porosity		Liquid velocity	Gas velocity Particle shape
Mechanical dispersion		Liquid velocity Gas velocity	Particle size	Particle shape Porosity
Capillary dispersion	Particle size Porosity	Liquid velocity Gas velocity		Particle shape

The phase interaction forces alone are sufficient for trickle-bed reactor modeling only when the flow is uniform radially. In more complicated situations, such as a point liquid source, the phase interaction forces fail to predict the extent of liquid spreading. Recently Atta et al. (2007) performed liquid dispersion simulations with CFD using a porous media concept without any additional dispersive forces. They compared the simulations to the experimental results of Herskowitz and Smith (1978) and Marcandelli (1999). The model performed well in the case of a multi-orifice liquid distributor. However, the simulation results for a single-orifice liquid distributor showed significant spreading only in the first case, where the column-to-particle diameter ratio was very low (~12) and a radial porosity profile was applied. In the latter case, where the column-to-particle diameter ratio was 150, the simulated liquid spreading was significantly less than the experimental one. It can be assumed that the modeled dispersion was mainly caused by wall flow and overloading. As a conclusion, the authors encouraged work on the incorporation of micro-scale details into macro-scale models for improved liquid dispersion predictions.

Simulations of liquid dispersion due to capillary pressure gradients have been reported, for example, by Boyer et al. (2005) and Jiang et al. (1999). As regards mechanical dispersion, CFD simulations have been performed for a tracer, where a separate convection-diffusion equation has been solved for the tracer phase (Gunjal et al. 2003a; Schnitzlein 2001; Yin et al. 2002). Prior to this work, there has not been a single CFD model for the mechanical dispersion of liquid. Hence various other approaches have been used thus far, including mathematical models (Prchlík et al., 1975), random walk methods (Barnett, 1975; Hoek et al., 1986; Maier et al., 2003; Marchot et al., 1992; Porter 1968; Sahimi et al., 1986a,b; Scott, 1935), network models (Herskowitz and Smith, 1978; Saroha et al., 1998), and automata models (Yang et al., 1998). In paper [I] we also presented an automata model for liquid flow simulations.

3. EXPERIMENTS

3.1 Trickle-bed experiments

The experimental set-up consisted of a rectangular column, gas and liquid distributors, and a liquid collector device. The column had a 25 cm x 5 cm cross-sectional area and its packed height could be altered from 25 to 100 cm. A schematic presentation of the set-up is presented in Figure 2. Gas and liquid were introduced into the column from the top and their flow rates were recorded with mass flow meters: Toshiba 191A5511 and Sensyflow eco, respectively. Gas was distributed to the column through two parallel pipes that both had 10 equidistant ø 4 mm orifices. The liquid distributor was alterable. The liquid flow was circulated to the liquid feed tank from the bottom of the column unless it was redirected to the liquid collector for flow rate measurements.

The bed was packed by slowly pouring the particles into the bed. The bed was also shaken from the sides to ensure the uniform packing of the particles. This also consolidated the bed to some extent. The packing density was determined by weighing. Measurements were started by first prewetting the bed with the Pseudo-Kan or Kan-prewetting method, depending on the circumstances. After prewetting, the gas flow rate was set to the desired value and the system was allowed to stabilize for about 20 minutes before measurements.

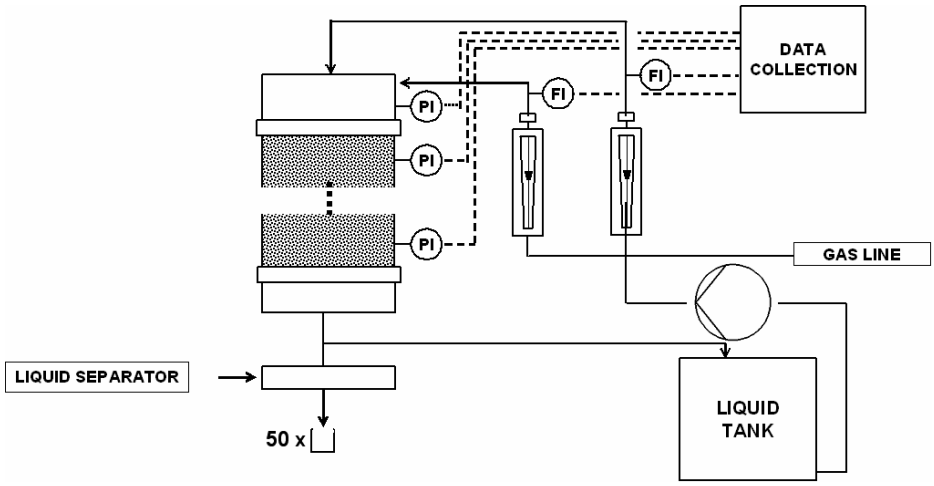

Figure 2. Schematic presentation of the experimental setup used in the trickle-bed experiments.

3.2 Standard deviation of porosity

The standard deviation of porosity describes how much the porous structure deviates from a uniform structure. In CFD modeling, standard deviation has been used to generate natural randomness in the generated porosity profile (Gunjal et al. 2005; Gunjal and Ranade 2007; Jiang et al. 2002). If used so, however, it should noted that the standard deviation should be dependent on the cell dimensions.

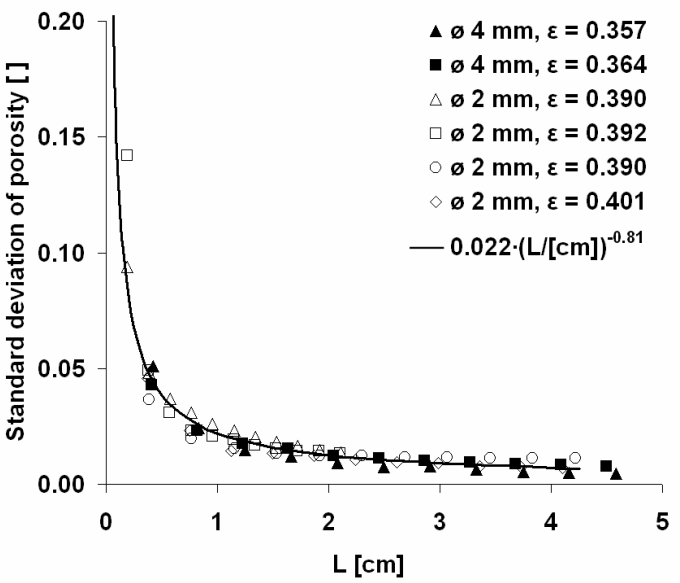

Figure 3. Effect of the experimental sample size on the standard deviation of porosity.

We used equipment similar to that presented by Borkink et al. (1992) to examine the dependence between the standard deviation of porosity and cell size. The equipment allowed us to measure the volume-averaged standard deviation, but unfortunately we could only change one dimension of the volume – the height. Two types of particles were used in the experiments: ø 2 mm and ø 4 mm glass spheres. From the results, it was observed that the particle size or the mean porosity did not significantly affect the standard deviation of porosity (the latter observation can also be seen from the results of Borkink et al. (1992)). Instead, it was found that the standard deviation of porosity was dominated by the height of the sample, L, as presented in Figure 3.

Based on these experiments, the volume-averaged standard deviation of porosity was estimated to depend on the sample height, L, which was the smallest dimension of the volume:

$$\sigma_\varepsilon = 0.022\left(\frac{L}{cm}\right)^{-0.805} \tag{1}$$

Borkink et al. (1992) obtained standard deviations between 0.032 and 0.057 for ø 9.7 mm spheres in a cylindrical bed with an inner diameter of 50 mm. The sample height in their measurements was approximately 0.5 cm. From equation (1) a standard deviation of 0.38 is obtained with L = 0.5 cm, which is consistent with the measurements of Borkink et al. (1992). Since the cross-sectional area of the bed in our experiments was more than 6 times greater than that in Borkink et al. (1992), it was concluded that the sample volume could not be the determining factor for the standard deviation, but that it should be the smallest dimension of the cell instead. This approach should be valid as long as cells contain both void spaces and particles.

4. HYDRODYNAMIC MODEL FOR TRICKLE-BED REACTORS

In computational fluid dynamics (CFD), the following conservation of mass and momentum equations are applied for gas and liquid phases in the case of gas-liquid flow through a porous medium:

$$\frac{\partial}{\partial t}(\theta_k \rho_k) + \nabla \cdot (\theta_k \rho_k \vec{u}_k) = 0 \tag{2}$$

$$\frac{\partial}{\partial t}(\theta_k \rho_k \vec{u}_k) + \nabla \cdot (\theta_k \rho_k \vec{u}_k \vec{u}_k) = \theta_k \mu_k \Delta \cdot \vec{u}_k - \theta_k \nabla p + \theta_k \rho_k \vec{g} + \vec{F}_{\text{int},k} + \vec{F}_{\text{disp},k} \tag{3}$$

Variables for phase *k* are the volume fraction, θ_k, density, ρ_k, viscosity, μ_k, and interstitial velocity, $\vec{u}_k$. Pressure, *p*, and the gravitational acceleration force, $\vec{g}$, are shared by all phases. The momentum source terms, $\vec{F}_{\text{int},k}$ and $\vec{F}_{\text{disp},k}$, refer to the total interaction force and to the total dispersion force for phase *k*, respectively.

4.1 The total interaction force

The total interaction force is a combination of gas-liquid, liquid-solid, and gas-solid phase interactions. It is written for gas and liquid phases as follows [III]:

$$F_{\text{int},G} = -f_e F_{GL} - (1 - f_e) F_{GS} \tag{4}$$

$$F_{\text{int},L} = f_e (F_{GL} - F_{LS}) \tag{5}$$

where F_{kj} is the phase interaction force between phases *k* and *j*. The wetting efficiency, f_e, describes the fraction of the catalyst surface covered with a flowing liquid film. The phase interactions are written as follows [II],[III]:

$$\vec{F}_{LS} = K_{LS} \vec{u}_L = \underbrace{\theta_L \left\{ \frac{E_{\mu,L}(1-\varepsilon)^2 \mu_L}{\theta_L^2 d_p^2} + \frac{E_{\rho,L}(1-\varepsilon)\rho_L |\vec{u}_L|}{\theta_L d_p} \right\}}_{K_{LS}} \vec{u}_L \tag{6}$$

$$\vec{F}_{GL} = K_{GL}(\vec{u}'_G - \vec{u}_L) = \underbrace{\theta_G \left\{ \frac{E_{\mu,G}(1-\theta_G)^2 \mu_G}{\theta_G^2 d_p^2} + \frac{E_{\rho,G}(1-\theta_G)\rho_G |\vec{u}'_G - \vec{u}_L|}{\theta_G d_p} \right\}}_{K_{GL}} (\vec{u}'_G - \vec{u}_L) \tag{7}$$

$$\vec{F}_{GS} = K_{GS} \vec{u}'_G = \underbrace{\theta_G \left\{ \frac{E_{\mu,G}(1-\theta_G)^2 \mu_G}{\theta_G^2 d_p^2} + \frac{E_{\rho,G}(1-\theta_G)\rho_G |\vec{u}'_G|}{\theta_G d_p} \right\}}_{K_{GS}} \vec{u}'_G \tag{8}$$

In equations (7) and (8), $\vec{u}'_G$ is the modified gas velocity. It is assumed that when liquid accumulates at the particle-particle contact points, the throats at the particle interstices become more and more narrow, resulting in a $1/\alpha$ times higher gas flow rate in these throats than the bed average. Since gas-liquid and liquid-solid phase interactions are thought to be confined in these throats, the gas velocity is modified [II].

Table 4. Summary of the experimental database used in the development of the tortuosity and wetting efficiency models.

Variable	Number of data points	Literature sources
Dimensionless pressure drop	252	Al-Dahhan and Duduković (1994); Iliuta et al. (1996); Iliuta and Thyrion (1997); Larachi et al. (1991); Specchia and Baldi (1977); Urseanu et al. (2005); Wammes et al. (1991)
Liquid saturation	405	Al-Dahhan and Duduković (1994); Burghardt et al. (1995); Colombo et al. (1976); Gladden et al. (2003); Iliuta et al. (1996); Iliuta and Thyrion (1997); Lakota and Levec (1990); Larachi et al. (1991); Levec et al. (1986); Pironti et al. (1999); Ring and Missen (1991); Specchia and Baldi (1977); Wammes et al. (1991)
Wetting efficiency	353	Al-Dahhan and Duduković (1995); Baussaron et al. (2007); Colombo et al. (1976); Kundu et al. (2003); Lakota and Levec (1990); Ring and Missen (1989); Ring and Missen (1991)

Table 5. Operation conditions of the measurements used in the model optimization.

	Pressure drop data	Holdup data	Wetting efficiency data
Temperature [K]	286 – 298	286 – 350	286 – 370
Pressure [bar]	1− 60	1− 100	1 − 100
Liquid density [kg/m^3]	663 − 1204	663 − 1204	651– 1000
Liquid viscosity [μPas]	307 − 35249	307 − 32723	292.1 – 1200
Gas density (operation conditions) [kg/m^3]	1.19 − 69.9	1.18 − 69.9	1.18 − 58.4
Gas viscosity [μPas]	17.0 − 19.5	14.2 − 19.5	14.0 − 18.4
Surface tension [N/m]	0.018 − 0.073	0.01 − 0.076	0.01 − 0.073
Particle diameter [mm]	1.14 − 5.4	1 − 6	1.0 − 7.3
Bed porosity [ ]	0.35 − 0.46	0.3 − 0.46	0.31 − 0.53
Liquid superficial mass flow rate [kg/(m^{2}s)]	0.63 − 15.0	0.09− 46.4	0.09 − 13. 7
Gas superficial mass flow rate [kg/(m^{2}s)]	0.01 − 7.7	0 − 7.7	0 − 4.2
Bed diameter [cm]	2.2 − 8.0	2.2 − 17.2	2.2 − 17.2

$$\vec{u}_G' = \vec{u}_G / \alpha \tag{9}$$

$E_{\mu,k}$ and $E_{\rho,k}$ are the phase-specific Ergun parameters. They account for the changes in the tortuosities experienced by gas and liquid due to the presence of the other phase in the spirit of the slit models (Holub 1990):

$$E_{\mu,k} = 72 T_k^2 \tag{10}$$

$$E_{\rho,k} = 6 f_\tau T_k^3 \tag{11}$$

The models for the liquid-solid wetting efficiency, f_e, and for the phase-specific tortuosities, T_L and T_G, were developed in papers [II] and [III] based on an experimental dataset, which is summarized in Table 4. The range of the operation parameters in this dataset is presented in Table 5.

4.1.1 Phase-specific tortuosity models

On the basis of the idea that tortuosity is dependent on phase volume fractions in the bed, phase-fraction-dependent tortuosity models were presented for gas and liquid phases in paper [II]. After some revision to the liquid phase tortuosity model, the following equations were introduced for gas and liquid tortuosities in paper [III]:

$$T_G = \frac{T_0 + 1}{2} + \alpha\left(\frac{T_0 + 1}{2} - 1\right) \tag{12}$$

$$T_L = T_0 A^{(\alpha^B)} \tag{13}$$

where parameters A and B are 3.592 and 1.140, respectively [III]. In principle, phase-specific tortuosities are affected by the presence of the second phase so that the tortuosity for the gas phase is always less than and the tortuosity for the liquid phase is always greater than the tortuosity in one-phase flow. This is consistent with trickle flow where liquid flows along the particles, whereas gas flows in the particle interstices. The empty bed tortuosity, T_0, and the friction factor, f_σ, can be calculated from the one-phase Ergun parameters according to equations (10) and (11).

4.1.2 Wetting efficiency model

Van de Merwe and Nicol (2005) identified three prewetting methods often used in experimental trickle-bed reactors:

- **Non-prewetted bed**
  Experiments are started off with an originally dry bed.
- **Levec-prewetted bed**
  The bed is flooded and then allowed to drain completely before experiments.
- **Kan-prewetted bed**
  Experiments are started off by operating the bed in a pulsing flow regime after which the gas and liquid flow rates are reduced to the desired values.
- **Pseudo-Kan-prewetted bed (referred to also as a super-prewetted bed by Loudon et al. 2006)**
  If a pulsing flow cannot be achieved (no gas feed or only local liquid feed), a pseudo-Kan-prewetted bed can be achieved by flooding the bed as in the Levec-prewetting method, but then commencing liquid flow simultaneously with draining; i.e. the column drains while under irrigation.

The selection of prewetting method has a significant effect on trickle-bed hydrodynamics. It has been found that flow is more uniform in a prewetted bed (Lutran et al. 1991; Ravindra et al. 1997; Sederman and Gladden 2001). Prewetting does not, however, guarantee uniform flow. Also, the prewetting method is significant: a Kan-prewetted bed is characterized by a film flow whereas a Levec-prewetted bed is characterized by a pore-rivulet flow surrounded by a film flow (van Houwelingen 2006; van Houwelingen et al.

2006; van de Merwe and Nicol 2005). It was reported in Van Houwelingen (2006) and van Houwelingen et al. (2006), that wetting efficiencies in Kan- and Levec-prewetted beds are different and that the difference is larger with low liquid velocities. Thus it was concluded in paper [III] that a wetting efficiency model should be fitted for a specific prewetting method.

The wetting efficiency model in paper [III] was developed for Kan-prewetted (Kan and Greenfield 1978), or equivalent, flow conditions. Since the hydrodynamic model is affected by the wetting efficiency model predictions, the wetting efficiency model was developed simultaneously with the hydrodynamic model. Thus, instead of simply considering how the wetting efficiency model performed as regards the wetting efficiency database, it was also considered how well the overall hydrodynamic model performed regarding the pressure drop and liquid saturation databases.

Since wetting efficiency is too complex a phenomenon to be modeled solely on phenomenological reasoning, a mechanistic model, based on dimensionless similitude, was used with some adjustable parameters. The dimensionless similitude enhances the predictive capabilities of the model, if used outside the realm of the experimental area used for fitting. The search for the optimal wetting efficiency model was begun with only one dimensional group. The number of dimensionless groups was then gradually increased, until the model provided a good fit to the experimental data and also reproduced properly all the known trends of wetting efficiency. The latter was considered significant if the model is to be used out of the operation range used in the model development. Details of the optimization process are reported in paper [III].

$$f_e = 0.335\,\mathrm{Re}_L'^{0.185}\mathrm{E\ddot{o}}'^{-0.188}\mathrm{Ga}_G'^{0.027}\left(1+\mathrm{Fr}_\mathrm{G}\right)^{-0.014} \tag{14}$$

4.2 Total dispersion forces

The total dispersion force for phase *k* is a combination of mechanical and capillary dispersion forces. The mechanical dispersion force is included for both phases, but the capillary dispersion is only included for one of the phases. Here the capillary dispersion force is included in the momentum equation of liquid.

4.2.1 Capillary dispersion

When immiscible fluids (e.g. gas and liquid) co-exist in a system of capillaries, such as porous media, the phases experience different pressures. The pressure difference is known as capillary pressure and is determined by the local curvature of the interface, R^*, and by the gas-liquid-solid surface tension, σ (e.g. Dullien 1992, pp. 120−121):

$$p_c = p_{nw} - p_w = \frac{2\sigma}{R^*} \tag{15}$$

where p_{nw} and p_w are the pressures of the non-wetting and the wetting phase, respectively. In trickle-bed reactors, gas is the non-wetting and liquid the wetting phase.

Capillary pressure changes as the relative saturation of the wetting and the non-wetting phases change. Thus experimental results are commonly reported as capillary pressure – saturation curves (e.g. Bradford and Leij 1995; Demond and Roberts 1991; Dodds and Srivastava 2006; Dullien et al. 1989; Leverett 1941). In CFD modeling, the capillary dispersion is implemented as a momentum source term for the liquid phase:

$$F_{Disp,L} = F_{cp,L} = \theta_L \nabla p_c \tag{16}$$

The capillary pressure curve can be divided into three regimes: pendular, funicular, and capillary. In trickle-bed reactors, the last-mentioned regime is rarely encountered, and thus a capillary pressure model suitable for trickle-bed reactor modeling needs to cover only the pendular and funicular regimes. In paper [IV] a capillary pressure model was developed for spherical particles for the pendular and funicular regimes. The model is based on an analytical analysis of the mean curvature of the meniscus. The filling angle at which the transition from the funicular to the pendular regime occurs is determined as follows:

$$p_{c,pend}(\varphi) = p_{c,fun}(\varphi) \leftrightarrow \varphi = \varphi_{tr} \tag{17}$$

Pendular regime

In the pendular regime, liquid is retained in pendular rings at the particle-particle contact points. The shape of a pendular ring is determined by the two principal radii R_1 and R_2, the particle radius R, the filling angle φ, and by the gas-liquid-solid contact angle θ (Figure 4):

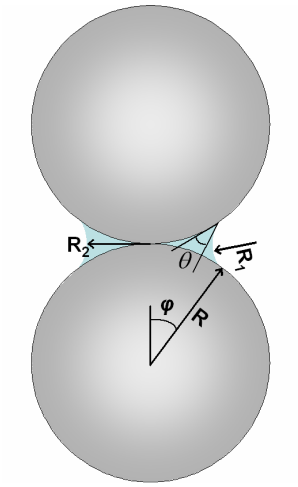

Figure 4. Schematic presentation of a pendular ring between two spherical particles, where R_1 and R_2 are the two principle radii, R is the particle radius, φ is the filling angle and θ is the gas-liquid-solid contact angle.

The analytical treatment of capillary pressure in the pendular regime is quite straightforward. The mean curvature of the radius, R^*, is obtained from the two principle radii, R_1 and R_2, as follows:

$$\frac{1}{R^*} = \frac{1}{2}\left(\frac{1}{R_1} + \frac{1}{R_2}\right) \tag{18}$$

If it is assumed that the liquid bridge has the form of a surface of revolution of a circular arc, equations (19) and (20) can be obtained for the two radii of curvature. In reality, the shape of the liquid bridge is nodoid, but the error caused by the toroidal approximation is less than 0.06 % (Mayer and Stowe 2005), which makes the use of the toroidal approach acceptable.

$$r_1 = \frac{(1-\cos\varphi)}{\cos(\varphi+\theta)} \tag{19}$$

$$r_2 = -\left[\sin\varphi - (1-\cos\varphi)\left(\frac{1}{\cos(\varphi+\theta)} - \tan(\varphi+\theta)\right)\right] \tag{20}$$

where $r_i = R_i / R$. In equation (15) capillary pressure is defined so that a curvature radius is positive if its center of curvature is on the non-wetting fluid side and negative if it is on the wetting fluid side.

The related liquid saturation can be obtained from the volume of liquid in the pendular ring, V_f:

$$S_L = \frac{3N_c(1-\varepsilon)}{\pi\varepsilon d_p^3}\cdot V_f \tag{21}$$

where S_L is liquid saturation, N_c is the number of particle-particle contact points for one particle, ε is bed porosity, d_p is particle diameter. The number of particle-particle contact points varies as the structure of packing changes. Usually the changes are related to bed porosity (German 1989; Haughey and Beveridge 1966; van der Merwe et al. 2004). Since small changes in the number of particle-particle contact points have a negligible effect on capillary pressure, a simple, linear correlation $N_c \propto 1/\varepsilon$ is used here. The correlation is similar to the one presented by German (1989) and it meets the contact points for simple cubic (*sc*) and face-centered cubic (*fcc*) packings with $N_c = 6$ and 12, respectively:

$$N_c = \frac{3.42}{\varepsilon} - 1.18; \quad \varepsilon_{fcc} \le \varepsilon \le \varepsilon_{sc} \tag{22}$$

Equations for the volume of liquid in a pendular ring have been derived by several authors (Dallavalle 1948, p. 288; Gardner and Gardner 1953; Gvirtzman and Roberts 1991; Likos and Lu 2004; Mayer and Stowe 1966; Rose 1958) with some discrepancies among them. In paper [IV] the following expression was presented:

$$V_f = 2\pi R^3 \left\{ \left[(r_1 - r_2)^2 + r_1^2 \right] X - r_1 (r_1 - r_2) \left[X \sqrt{1 - \left(\frac{X}{r_1} \right)^2} + r_1 \arcsin\left(\frac{X}{r_1} \right) \right] - X^2 \right\} \quad (23)$$

where $X = (1 - \cos\varphi)$. The expression is consistent with the expressions of Mayer and Stowe (1966) and Likos and Lu (2004) for all contact angles. In the case of θ = 0 the expression is also consistent with the expression of Rose (1958), in which case equation (23) is notably simplified:

$$V_{f,\theta=0} = 2\pi R^3 \left\{ r_1^2 \left[1 - (r_1 - r_2)(\pi/2 - \varphi) \right] \right\} \quad (24)$$

Since capillary pressure and liquid saturation can be both written as functions of the filling angle, the relation between them can be expressed as follows:

$$p_c(\varphi) = \frac{2\sigma}{2} \left(\frac{1}{R_1(\varphi)} + \frac{1}{R_2(\varphi)} \right) \leftrightarrow S_L(\varphi) = \frac{3N_c(1-\varepsilon)}{\pi \varepsilon d_p^3} \cdot V_f(\varphi) \quad (25)$$

Funicular regime

In the funicular regime, capillary pressure is different in drainage and imbibition. The operation conditions in a trickle-bed reactor are equivalent to drainage, and thus imbibition is not considered here. Capillary pressure in the funicular regime, in a drainage situation, has been found to be governed by the smallest openings at particle interstices (Dullien et al. 1989; Novy et al. 1989). If the particle size and the porosity of packing are constant, which corresponds to an ideal packing, the capillary pressure in the funicular regime is also constant and corresponds to a transitional capillary pressure. Transitional capillary pressure refers to the capillary pressure at the transition point from the funicular to the pendular regime [IV]. A similar assumption has also been made by Carman (1956, p. 40). Thus the capillary pressure in the funicular regime was determined based on the liquid structures at the transition point from the funicular to the pendular regime. This is presented in Figure 5 for a simple cubic (*sc*) packing and for a face-centered cubic (*fcc*) packing.

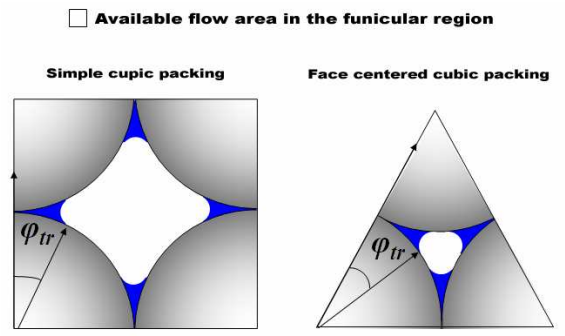

Figure 5. Illustration of the available openings at the transition point from the funicular to the pendular regime in the case of a simple cubic (left) and face-centered cubic (right) packing.

The hydraulic diameters corresponding to the openings presented in Figure 5 are calculated from the cross-sectional area, $A_{c,i}$, and the wetted perimeter, s_i, of the flow channel:

$$D_{H,i} = \frac{4A_{c,i}}{s_i} \tag{26}$$

Since the calculation of the hydraulic diameter requires the knowledge of pore structure, it cannot be solved analytically for all porosities. It is thus assumed that if the porosity is ε_{sc} or ε_{fcc}, the pore structure will correspond to a simple cubic (*sc*) or to a face-centered cubic (*fcc*) packing, respectively. Then for a simple cubic (*sc*) and a face-centered cubic (*fcc*) packing the cross-sectional area, $A_{c,i}$, is calculated as follows:

$$A_{c,sc} = d_p^2 - \frac{1}{4}\pi d_p^2 - 2A_{c,f,tr} \tag{27}$$

$$A_{c,fcc} = \frac{d_p^2\sqrt{3}}{4} - \frac{1}{8}\pi d_p^2 - \frac{3}{2}A_{c,f,tr} \tag{28}$$

where $A_{c,f,tr}$ is the cross-sectional area of liquid in a pendular ring at the funicular-to-pendular transition point [IV]. $A_{c,f,tr}$ is calculated with the transition filling angle, φ_{tr}:

$$\begin{aligned}\frac{A_{c,f,tr}}{R^2} = {} & 4\left(r_{1,tr} - r_{2,tr}\right)X_{tr} - 2r_{1,tr}X_{tr}\sqrt{1-\left(\frac{X_{tr}}{r_{1,tr}}\right)^2} \\ & - 2r_{1,tr}^2 \arcsin\left(\frac{X_{tr}}{r_{1,tr}}\right) - \left(2\varphi_{tr} - \sin 2\varphi_{tr}\right)\end{aligned} \tag{29}$$

The length of the wetted perimeter is calculated for *sc*- and *fcc*-packing as follows:

$$s_{sc} = R\left[4\left(\frac{\pi}{2} - 2\varphi_{tr}\right) + 4\left(\pi - 2\varphi_{tr} - 2\theta\right)r_{1,tr}\right] \tag{30}$$

$$s_{fcc} = R\left[3\left(\frac{\pi}{3} - 2\varphi_{tr}\right) + 3\left(\pi - 2\varphi_{tr} - 2\theta\right)r_{1,tr}\right] \tag{31}$$

The hydraulic diameter can then be calculated for these two porosities. The function between the hydraulic diameter and porosity is obtained by assuming a linear dependency between them:

$$D_H = D_{H,sc} - \left(\frac{\varepsilon_{sc} - \varepsilon}{\varepsilon_{sc} - \varepsilon_{fcc}}\right)\left(D_{H,sc} - D_{H,fcc}\right) \tag{32}$$

The capillary pressure is finally obtained from equation (15) with $R^* = D_H/2$.

Sequential variables

In the above, a uniform pore structure, particle size and porosity have been assumed. In real applications, however, the packing structure is rarely uniform, and there is some variance in the particle size and porosity. These variations cause gas to replace liquid sequentially, starting from the largest pores and graduating to the smallest pores. The concept of sequential draining is consistent with the basic assumptions behind pore-size distribution measurements based on capillary pressure (Carman 1956, pp. 39−41).

The local pore size is linked to the local values of porosity and particle size – if the local porosity and/or particle size are larger than the bed average, the pore size adjacent to them is also likely to be larger than the average, and vice versa. Thus the concepts of sequential porosity ε_{seq} and sequential particle diameter $d_{p,seq}$ are used to characterize the pore size to be drained next.

For modeling purposes the sequential variables are required as functions of S_L. The connection between liquid saturation and sequential variables is developed on the basis of the following reasoning. At high liquid saturation, sequential behavior will cause the gas to replace liquid first in places with large pores i.e. in places where sequential porosity and/or particle size are larger than the average. Consequently, the sequential porosity and particle size should obtain the largest values at liquid saturations close to one. As liquid saturation decreases, gas starts to replace liquid from smaller and smaller pores. Thus sequential particle size and porosity should be decreasing functions of liquid saturation. Finally, at liquid saturations close to zero, the liquid phase is mostly confined in the pendular rings. Since smaller particles imply higher capillary pressure, the last remainder of the liquid will be found in the contact points of the smallest particles.

Sequential porosity

The density distribution of porosity in a packed bed is assumed to follow the beta distribution function within the interval [ε_{min}, ε_{max}]:

$$f(\varepsilon)=\frac{\Gamma(p'+q')}{\Gamma(p')\Gamma(q')(\varepsilon_{\max}-\varepsilon_{\min})}\left(\frac{\varepsilon-\varepsilon_{\min}}{\varepsilon_{\max}-\varepsilon_{\min}}\right)^{p'-1}\left(\frac{\varepsilon_{\max}-\varepsilon}{\varepsilon_{\max}-\varepsilon_{\min}}\right)^{q'-1} \tag{33}$$

The parameters p' and q' are chosen so that the distribution mean and variance correspond to that of the packed bed, i.e. $\bar{\varepsilon}$ and σ_ε, respectively. The theoretical boundary values for $\varepsilon_{\min}$ and $\varepsilon_{\max}$ are 0.2595 (for ideal dense packing) and 1, respectively. The use of these values will, however, result in a density function with long tails that consists of values that are effectively zero. It is thus profitable to choose ε_{min} and ε_{max} so that the shape of the distribution is maintained, but the tails of the distribution are cut off at the proper locations. This can be done by limiting the values of p' and q' to the maximum value of $p'_{\max}$. The maximum and minimum porosities can be then obtained from the following equations:

$$\varepsilon_{\min}=\max\left(0.2595;\bar{\varepsilon}-\sigma_\varepsilon\sqrt{2p'_{\max}+1}\right) \tag{34}$$

$$\varepsilon_{\max}=\min\left(1;\bar{\varepsilon}+\sigma_\varepsilon\sqrt{2p'_{\max}+1}\right) \tag{35}$$

It must be emphasized that when $p'_{\max}$ is chosen so that the density function will reach zero at both ends, the final porosity distribution function is not affected.

The relation between sequential porosity and liquid saturation can be calculated as follows:

$$S_L(\varepsilon_{seq}) = \frac{1}{\bar{\varepsilon}} \int_{\varepsilon_{\min}}^{\varepsilon_{seq}} \varepsilon \cdot f(\varepsilon) \mathrm{d}\varepsilon \tag{36}$$

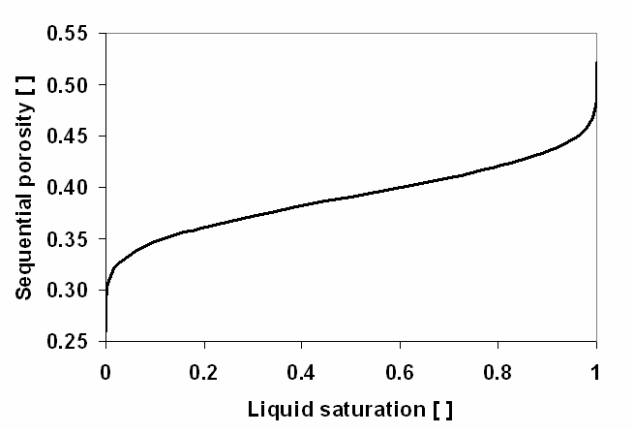

Figure 6. Sequential porosity as a function of liquid saturation. Mean porosity is 0.39 and σ_ε is 0.034 based on equation (57). P_{max} is set to 7.

The effect of the remaining pendular rings on equation (36) is considered insignificant. The average volume of liquid in pendular rings at the transition point is about 4 and 6 percent of the total pore volume for smooth and rough particles, respectively. Thus the volume of the remaining pendular rings at the particle contact points is small when compared to the volume of the liquid at the funicular structures. An example of the sequential porosity as a function of liquid saturation is presented in Figure 6.

Sequential particle size

A simple power equation was assumed to suit the sequential particle size − the liquid saturation correlation in the case of uniform particle size distribution.

$$d_{p,seq} = d_{p,\min} + \Delta d_p S_L^n \tag{37}$$

The value for the power *n*, was determined empirically based on the capillary pressure – liquid saturation data of Dodds et al. (2006) [IV].

$$n = \Delta d_p / \bar{d}_p; \quad \Delta d_p = d_{p,\max} - d_{p,\min} \tag{38}$$

Although the capillary pressure model was developed under an assumption of a uniform particle size distribution, its applicability was also tested for the capillary pressure data Dodds et al. (2006) had measured for mixtures of three particle sizes. The shape of the $d_{p,seq}$ function was obtained on the basis of the data. It was found that the smallest particle size determined the capillary pressure in the pendular regime. In the funicular regime a correlation similar to equation (37) was used, where d_{p1}, d_{p2} and d_{p3} are the three particle sizes in the mixture, d_{p1} being the smallest and d_{p3} the largest.

$$d_{p,seq} = \begin{cases} d_{p1} & S_L \le S_{L,tr} \\ d_{p,\min} + \Delta d_p \left(\dfrac{S_L - S_{L,tr}}{1 - S_{L,tr}} \right)^{1-\frac{d_{p2}}{d_{p3}}} & S_L > S_{L,tr} \end{cases} \tag{39}$$

Capillary pressure curve for CFD

The capillary pressure model, described above, gives the relation between capillary pressure and liquid saturation. Capillary pressure cannot, however, be written explicitly as a function of liquid saturation i.e. as $p_c = f(S_L)$. Thus an analytical fit is beneficial before the capillary pressure model can be implemented in CFD. Here we have used the following type of equations in the pendular and funicular regimes:

$$\frac{p_{c,pend} R}{\sigma} = k_0 + k_1 S_L^{k_2} + \frac{k_3}{S_L^{k_4}}, \quad S_L < 0.9 S_{L,tr} \tag{40}$$

$$\frac{p_{c,fun} R}{\sigma} = k_5 + k_6 S_L^{k_7} + k_8 S_L^{k_9}, \quad S_L > 1.1 S_{L,tr} \tag{41}$$

where $S_{L,tr}$ is the liquid saturation at φ_{tr}, i.e. at the point where the transition from the funicular to the pendular regime occurs. Since the capillary pressure function and its derivative have to be continuous, a third order polynomial is used between the two regimes:

$$\frac{p_{c,fit} R}{\sigma} = k_{10} + k_{11} S_L + k_{12} S_L^2 + k_{13} S_L^3, \quad 0.9 S_{L,tr} < S_L < 1.1 S_{L,tr} \tag{42}$$

The parameters k_i are fitted for each case separately based on $P_c - S_L$ pairs that are solved iteratively from the capillary pressure model. The limits and the parameters of the polynomials are chosen so that the capillary pressure curve shifts smoothly between the pendular and funicular regimes and both the capillary pressure curve and its gradient are continuous functions of S_L.

4.2.2 Mechanical dispersion

Mathematically, the mechanical dispersion of tracer is quite a well-understood phenomenon and can be described similarly to molecular dispersion using a standard macroscopic convection-diffusion equation. The mechanical dispersion of liquid is, however, more complicated and there are a few unanswered questions in connection with

it. First of all, in Figure 7 it is demonstrated that in the case of a liquid source feed, the mechanical dispersion force is not the only force affecting liquid spreading. Thus in liquid source feed dispersion experiments, mechanical dispersion cannot be separated from the other phenomena affecting spreading and the spread factor should be considered as a net spread factor, including, at the minimum, the effect of the phase interaction forces. It might also be affected by overloading and/or capillary spreading. Secondly, in liquid dispersion, the velocity of liquid is not constant, but also has a distribution, whereas in tracer dispersion the velocity in equation (55) is constant. Therefore, although on some occasions similar values have been obtained for spread factors from tracer and liquid dispersion experiments (Herskowitz and Smith, 1978), it does not follow that the values should necessarily be the same. Below the discrepancies are considered, based on CFD modeling.

Tracer dispersion model

A key assumption behind tracer dispersion experiments is that the physical properties of the tracer can be considered identical with those of the bulk liquid phase. In other words it is assumed that the presence of the tracer will not affect the hydrodynamics of the flow. Thus tracer dispersion can be modeled in CFD with a separate scalar transport equation for species. This results in the following standard macroscopic convection-diffusion equation that is solved for the tracer phase (Yin et al., 2002; Gunjal et al., 2003):

$$\frac{\partial \theta_L \rho_L Y_{i,L}}{\partial t} + \nabla \cdot \left(\theta_L \rho_L \vec{u}_L Y_{i,L} \right) = \nabla \cdot \left(\theta_L \rho_L \vec{D} \nabla Y_{i,L} \right) \tag{43}$$

where Y_i is the mass fraction of component i in the bulk phase and θ_k and ρ_k denote the phase fraction and density of phase k respectively. The applicability of such a convection-diffusion equation on tracer dispersion has been discussed and confirmed in Porter (1968) and Sahimi et al. (1986a,b), and the references therein.

Most of the commercial CFD programs include a species transport model and the user is required simply to add the diffusion coefficient, $D = D_m + D_{mech}$, which simplifies to the mechanical dispersion coefficient: $D = D_{mech}$ with a high enough Péclet number (Coelho and Guedes de Carvalho 1988; Ligny 1970).

Liquid dispersion model

A model for the mechanical dispersion of liquid was presented in paper [V]. Since the standard multiphase equations solved in CFD are derived using mass-weighted averaging of instantaneous local equations, diffusion-type terms do not appear in the continuity equations. Instead, the correct way to introduce diffusion is to add dispersion forces into the momentum equations. This can be understood on the basis that momentum is also transferred in a multiphase dispersion.

The hydrodynamic dispersion results from the velocities perpendicular to the main flow caused by the tortuous bed structure. The dispersive force is obtained by multiplying this lateral drift velocity by the appropriate momentum exchange coefficient. Assuming that the x-axis is perpendicular to the main flow direction, the dispersion forces in the x-direction can be written as presented in equations (44) and (45).

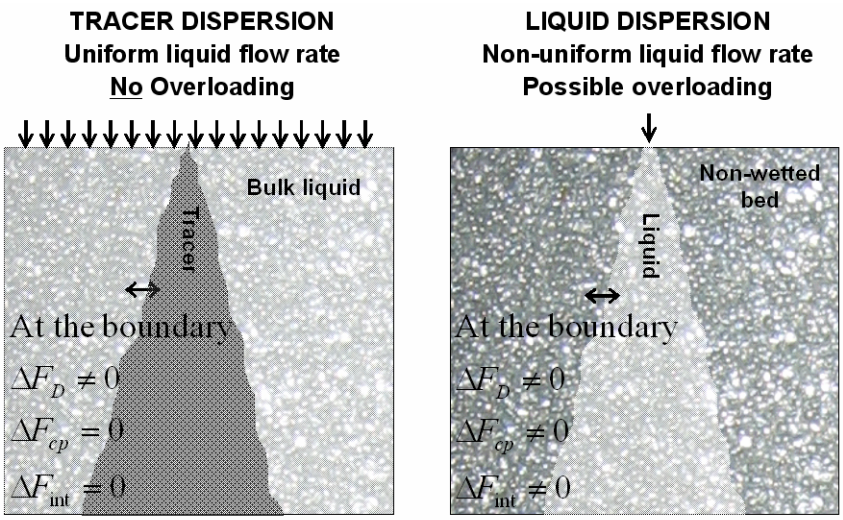

Figure 7. Forces affecting spreading in case of liquid and tracer dispersion in trickle-bed reactors.

$$F_{D_x,G} = (1-f_e)K_{GS}u_{D_x,G} + f_e K_{GL}\left(u_{D_x,G} - u_{D_x,L}\right) \tag{44}$$

$$F_{D_x,L} = f_e K_{LS}u_{D_x,L} - f_e K_{GL}\left(u_{D_x,G} - u_{D_x,L}\right) \tag{45}$$

where K_{LS}, K_{GL} and K_{GS} are the momentum exchange coefficients in equations (6) – (8) and $u_{D_x,k}$ is the *x*-component of the drift velocity $\vec{u}_{D,k}$ for phase *k*. The form of $F_{D_x,k}$ is exactly the same as that of $\vec{F}_{\text{int},k}$ in (4) and (5). The symmetry with respect to the liquid and gas phases ensures that the liquid dispersion does not result in a net force on the system. The gas-solid and liquid-solid forces are balanced by the immobile solid phase.

The drift velocities are defined by writing the diffusion mass flux as $\theta_k \rho_k u_{D_x,k}$. Based on the Fickian assumption, the drift velocities are then obtained from the following expressions:

$$u_{D_x,G} = -\frac{S\left|u'_{\parallel,G}\right|}{\theta_G}\frac{\partial \theta_G}{\partial x} \tag{46}$$

$$u_{D_x,L} = -\frac{S\left|u_{\parallel,L}\right|}{\theta_L}\frac{\partial \theta_L}{\partial x} \tag{47}$$

where $u'_{\parallel,G}$ is the part parallel to the main flow of the modified gas velocity that was defined in equation (9) and *S* is the spread factor.

The above model for mechanical dispersion has been used in papers [V] and [VI]. The model can, however, be generalized for the case where liquid flow is not parallel to the main flow. In this case drift velocity should be proportional to the projection of the gradient of the volume fraction to the plane orthogonal to the liquid velocity. From the

geometrical consideration in 2D and 3D, the following expressions can be obtained for the drift velocities of gas and liquid:

$$\mathbf{u}_{D,L} = -\frac{\hat{S}}{\theta_L}\left[|u_L| \nabla\theta_L - (\mathbf{u}_L \cdot \nabla\theta_L)\frac{\mathbf{u}_L}{|u_L|} \right] \tag{48}$$

$$\mathbf{u}_{D,G} = -\frac{\hat{S}}{\theta_G}\left[|u'_G| \nabla\theta_G - (\mathbf{u}'_G \cdot \nabla\theta_G)\frac{\mathbf{u}'_G}{|u'_G|} \right] \tag{49}$$

In the general case the structure of the dispersion forces remain the same as in equations (44) and (45). In the cases simulated in papers [V] and [VI], the vertical flow was dominant. Since the generalized model coincides with the previous one if the flow has only one direction, the results with the general model differ only slightly from the current results.

5. MODEL VALIDATION

5.1 Phase interaction model

The two-phase pressure drop model was validated against the experimental data presented in Table 4. In addition, its performance has been compared to the performance of other literature models [III]. The performance of the models was evaluated on the basis of a selection of statistical numbers, which are presented below.

The mean relative error describes the overall exactness of the fit between the model predictions and the experimental results. The following expression is used for $\langle e_X \rangle$, where $1+X_{\exp,i}$ is used as a denominator to prevent the over-emphasis of the smallest measured values.

$$\langle e_X \rangle = \frac{100\%}{N} \sum_{1}^{N} \left| \frac{X_{\exp,i} - X_{calc,i}}{1 + X_{\exp,i}} \right| \tag{50}$$

The sum of all errors is used to examine whether the model is biased. For an unbiased model $B(X)$ should be close to zero.

$$B(X) = \frac{1}{N} \sum_{1}^{N} \left(X_{\exp,i} - X_{calc,i} \right) \tag{51}$$

The standard deviation of the relative error around the mean relative error, STD_e, can be used to compare the ability of the models to describe correctly the trend of the modeled property.

$$STD_e = 100 \cdot \sqrt{\frac{1}{N-1} \sum_{1}^{N} \left(\left| \frac{X_{\exp,i} - X_{calc,i}}{1 + X_{\exp,i}} \right| - \langle e_X \rangle \right)^2} \tag{52}$$

5.1.1 Pressure drop and liquid holdup

By assuming a one-dimensional flow, steady-state operation, and no mass transfer between phases, the two-phase pressure drop and liquid holdup can be solved from the simplified momentum balances for gas and liquid [II]

$$\frac{\Delta P}{\Delta L} = \rho_L g + \frac{F_{\text{int},L}}{\theta_L} \tag{53}$$

$$\frac{\Delta P}{\Delta L} = \rho_G g + \frac{F_{\text{int},G}}{\theta_G} \tag{54}$$

where $F_{int,k}$ is calculated from the phase interaction forces (equations (6)–(8)). The model parameters were optimized against 252 dimensionless pressure drop and 405 liquid saturation data points (see Table 4) in paper [III]. Much of the research on trickle-bed

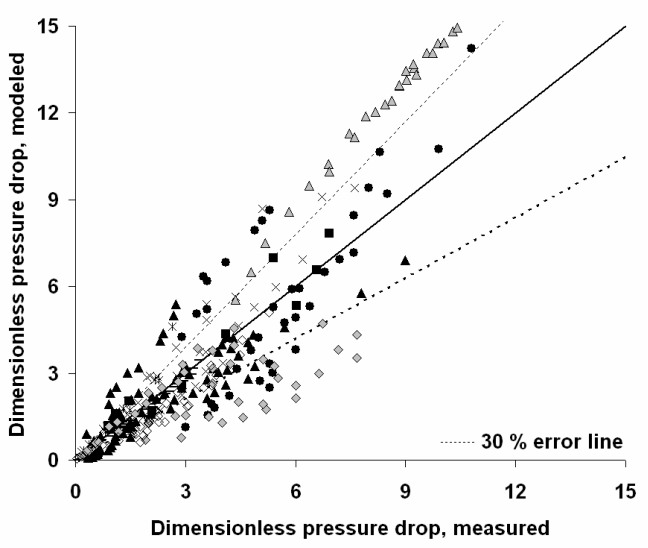

Figure 8. Parity plot between the modeled and measured dimensionless pressure drops. Data used in the optimization: (▲) Al-Dahhan and Duduković (1994), (×) Iliuta et al. (1996), (◇) Iliuta and Thyrion (1997), (●) Larachi et al. (1991), (✳) Specchia and Baldi (1997), (–) Urseanu et al. (2005), and (■) Wammes et al. (1991). Additional data: (△) Clements and Schmidt (1980), (◈) Rao et al. (1983).

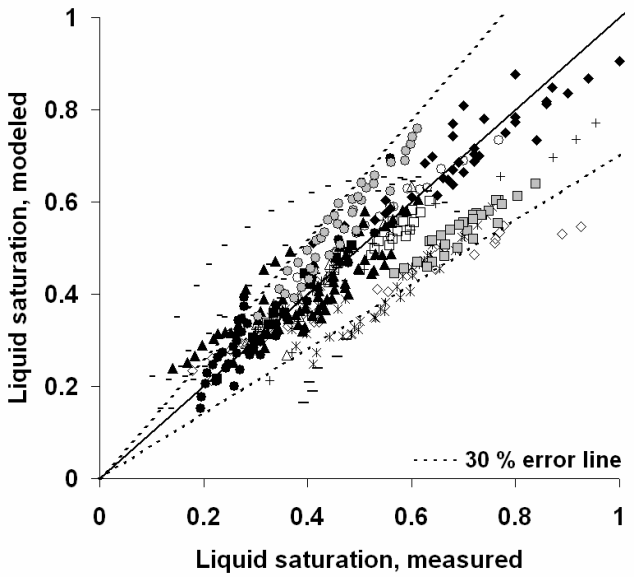

Figure 9 . Parity plot between the modeled and measured liquid saturations. Data used in the optimization: (▲) Al-Dahhan and Duduković (1994), (✳) Burghardt et al. (1995), (+) Colombo et al. (1976), (◇) Gladden et al. (2003), (○) Iliuta et al. (1996), (◍) Iliuta and Thyrion (1997), (△) Lakota and Levec (1990), (◆) Larachi et al. (1991), (-) Levec et al. (1986), (□) Pironti et al. (1999), (–) Ring and Missen (1991), (●) Specchia and Baldi (1997), (■) Wammes et al. (1991). Additional data: (×) Clements and Schmidt (1980).

hydrodynamics has been performed at atmospheric pressure, in a small column with a low column to particle diameter ratio without proper mention of the prewetting method. This makes the collection of a dataset for model development quite challenging, since the same operational parameters can result in various different hydrodynamic states (Loudon et al. 2006). The problem is more significant in the case of pressure drop, when the affect can be manifold. In the current study, the experimental database was chosen so that it would contain a significant amount of non air-water, above atmospheric pressure, large enough column-to-particle diameter ratio data. Multiple suggestions for sufficient column-to-particle diameter ratios have been offered in the literature (Saroha et al. 1998). Westerterp and Wammes (2005) set 15 as a rule of thumb value for the wall flow to be insignificant. In pressure drop and liquid saturation databases the column-to-particle diameter ratio is over 10 for 98 % and over 15 for over 60 % of both databases. Almost 50 % of the pressure drop and over 30 % of the liquid saturation experiments were performed at higher than atmospheric pressure. Close to 70 % of the pressure drop and close to 50 % of the liquid saturation experiments were performed with systems other than air/water. The performance of the optimized model is compared to the models of Attou et al. (1999), Tung and Dhir (1988), and Sáez and Carbonell (1985) in Table 6.

Table 6 Comparison of the performance of the current model to the models of Attou et al. (1999), Tung and Dhir (1988), and Sáez and Carbonell (1985) based on dimensionless pressure drop, $\Delta p/\Delta L$, and liquid saturation, S_L, data presented in Table 4.

	Current model	Attou et al. (1999)	Tung and Dhir (1988)	Sáez and Carbonell (1985)
$\langle e_{\Delta P/\Delta L} \rangle$	18.73	26.82	27.86	21.76
$STD_{e,\Delta P/\Delta L}$	15.65	14.26	15.07	12.72
$B(X)_{\Delta P/\Delta L}$	0.029	1.023	1.069	0.336
$\langle e_{S_L} \rangle$	5.43	8.62	7.92	7.07
STD_{e,S_L}	6.15	6.84	7.19	6.91
$B(X)_{S_L}$	0.017	0.094	0.083	0.079

Parity plots for the dimensionless pressure drop and liquid saturation data are presented in Figure 8 and Figure 9, respectively. The parity plots include all the data used for the optimization, as well as some additional data. The model predicts both trends quite well. Considering the complicated nature of the trickle-bed hydrodynamics (e.g. the hysteresis effect) the model performance, based on Table 6, Figure 8, and Figure 9, can be considered good.

5.1.2 Wetting efficiency

5.1.2.1 Performance of the wetting efficiency model

The validation of the wetting efficiency model was done against a large dataset. Part of the data was used in the model optimization (Al-Dahhan and Duduković 1995; Baussaron et al. 2007; Colombo et al. 1976; Kundu et al. 2003; Lakota and Levec 1990; Ring and Missen 1989; Ring and Missen 1991), but it also included data that was excluded from the

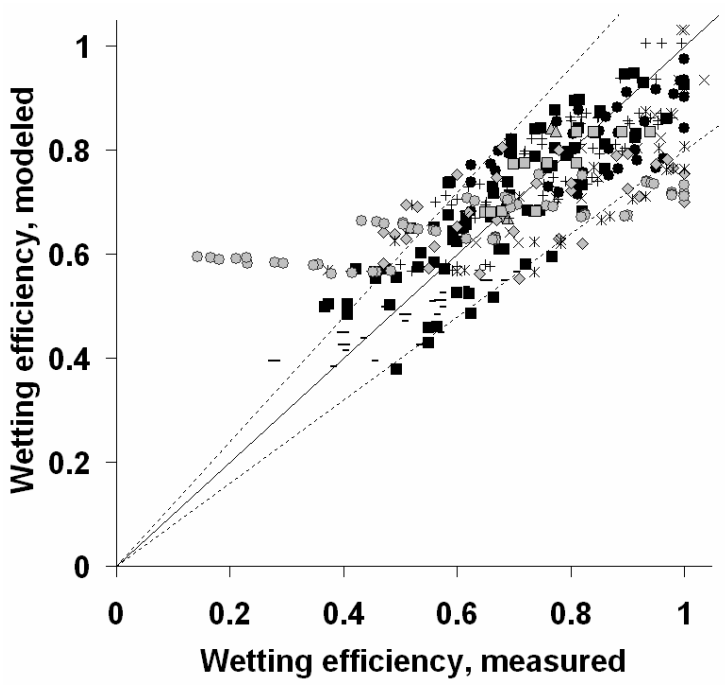

Figure 10. Parity plot between the modeled wetting efficiencies and literature data. Data used in the optimization: (•) Al-Dahhan and Duduković (1995), (■) Baussaron et al. (2007), (×) Colombo et al. (1976), (+) Kundu et al. (2003), (⋆) Lakota and Levec (1990), (-) Ring and Missen (1989), and (–) Ring and Missen (1991). Additional data: (⍟) Alicilar et al. (1994), (▲) van Houwelingen et al. (2006), (▫) Lazzaroni et al. (1988), and (◈) Specchia et al. (1978).

Table 7. Comparison of the performance of equation (14) to literature wetting efficiency correlations.

	$\langle e_{f_e} \rangle$	STD_{e,f_e}	$B(X)_{f_e}$	Applicability to the data [%]
New model	5.65	5.35	0.00	100.00
Alicilar et al. (1994)	26.14	8.20	0.56	13.88
Burghardt et al. (1995)	13.43	8.17	0.27	81.59
El-Hisnawi et al. (1982)	6.50	6.16	-0.10	100.00
González-Mendizibal et al. (1998)	17.32	7.28	0.41	25.50
Herskowitz (1981)	10.68	9.22	-0.30	100.00
Herskowitz and Smith (1983)	11.33	9.51	-0.33	100.00
Larachi et al. (2001)	8.56	7.94	-0.10	100.00
Mills and Duduković (1981)	10.78	9.21	-0.32	100.00
Ring and Missen (1991)	10.97	7.28	0.21	58.07

optimization dataset (Alicilar et al. 1994; van Houwelingen et al. 2006; Lazzaroni et al. 1988; Specchia et al. 1978) due to unknown porosity. When the data was used in the model validation, the porosity was estimated with the correlations presented in Bey and Eigenbergen (1997). The parity plot between the calculated and measured wetting efficiencies is presented in Figure 10. The correspondence between the predicted and measured values is good and most of the predicted wetting efficiencies are within the 20 % error line.

The performance of the wetting efficiency model was compared against the literature models of Alicilar et al. (1994), Burghardt et al. (1995), El-Hisnawi et al. (1982), González-Mendizibal et al. (1998), Herskowitz (1981), Herskowitz and Smith (1983), Larachi et al. (2001), Mills and Duduković (1981), Ring and Missen (1991). The results are presented in Table 7. The applicability of some models to the data was limited by the gas and/or liquid flow rates (see Table 2 for details). This is also indicated in Table 7. The current model showed improvement with respect to all the calculated statistical numbers.

The performance of the current model is also demonstrated in Figure 11, which presents the parity plots of the top four wetting efficiency models according to the statistical numbers in Table 6. It can be seen that the phenomenological models of El-Hisnawi et al. (1982) and Herskowitz (1981) have a tendency to overpredict wetting efficiency; especially as the wetting efficiency decreases. The parity plot of the neural network model of Larachi et al. (2001) is widely scattered. The current model seems to reproduce the trend most accurately.

Characteristics of the wetting efficiency model

In addition to the quantitative performance analysis presented above, the qualitative analysis of the model is also important, since it reveals whether or not the model reproduces the known characteristics of wetting efficiency. This is important since experimental data points are often obtained in small-scale equipment with moderate pressures and temperatures, but the model should be extendable to large-scale, high-pressure, and high-temperature industrial applications. The factors affecting the modeled wetting efficiency can be divided into four groups: liquid phase properties (U_L, ρ_L, μ_L), gas phase properties (U_G, ρ_G, μ_G), gas-liquid surface tension (σ), and bed properties (ε, d_p).

Liquid phase properties. Of the liquid phase properties only the effect of liquid velocity on wetting efficiency has been studied. The model is consistent with the majority of the available research, predicting a strong positive influence of liquid velocity on wetting efficiency. The model also predicts that an increase in liquid viscosity decreases wetting efficiency significantly.

Gas phase properties. The model predicts a contradictory effect of gas velocity on wetting efficiency: an increase in gas velocity decreases wetting efficiency, but at the same time the pressure drop increases, which in turn has a positive effect on wetting efficiency through increased gas density. This observation could explain the inconsistent conclusion made from the experimental results [III]. The effect of gas velocity is small. Change in gas density has a stronger effect, especially if the gas density is low.

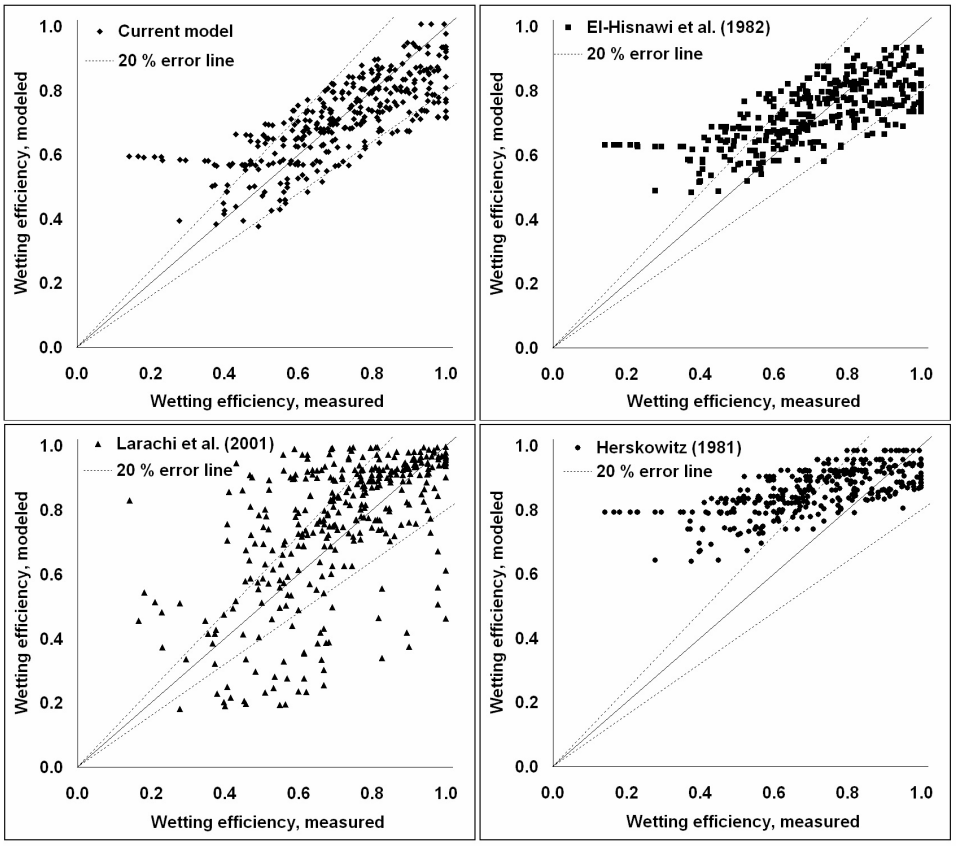

Figure 11. Comparison between the parity plots of the four top wetting efficiency models based on statistical numbers presented in Table 6.

Gas-liquid surface tension. Experimental results concerning the effect of the gas-liquid surface tension on wetting efficiency are scarce. The only results found are from the work of El-Hisnawi et al. (1982), who ascertained that surface tension had a positive effect on wetting efficiency. This is consistent with the predictions of the model.

Bed properties. The model predicts an increase in wetting efficiency as particle size or bed porosity decreases. This is consistent with the experiments of Baussaron et al. (2007) and also with the theoretical considerations of increased capillary dispersion [V].

5.2 Dispersion models

5.2.1 Capillary pressure model

The capillary pressure model was validated against the experimental data of Dodds and Srivastava (2006) and Dullien et al. (1989). In addition, the model performance was compared to the models of Attou and Ferschneider (2000) and Grosser et al. (1988). Figure 12 gathers the experimental results of Dodds and Srivastava (2006), with mono-sized particles, and the predictions of the three models. All three models perform qualitatively similarly in the funicular regime. The main differences can be found in the

pendular regime, where the capillary pressure rises steeply. For capillary dispersion this is the most significant regime, since the steep rise in capillary pressure implies large capillary pressure gradients. From Figure 12 it can be seen that the current model significantly improves the capillary pressure prediction in the pendular regime when compared to the model of Grosser et al (1988). The model of Attou and Ferschneider (2000) was developed for the funicular regime only.

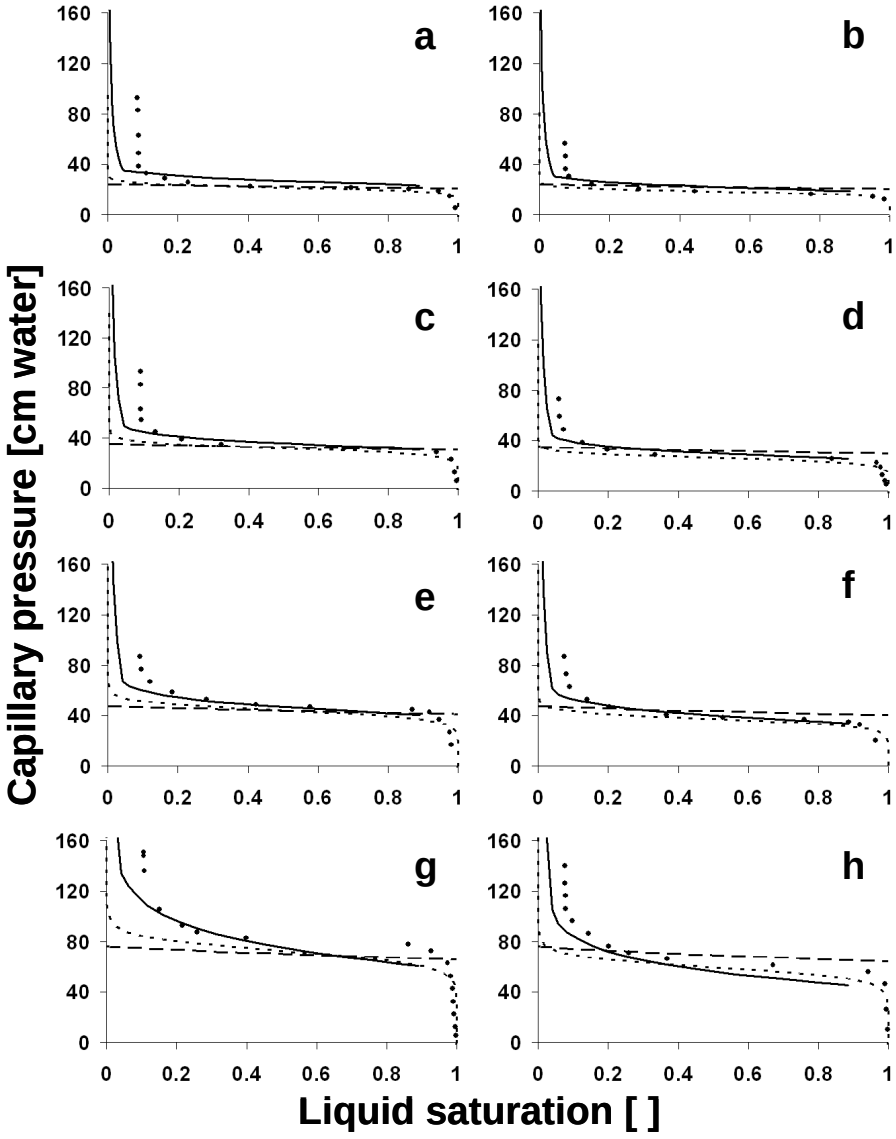

Figure 12. Comparison between the models and the experiments with beds packed with mono-sized particles. — the new capillary pressure model, ···· the model of Attou and Ferschneider (2000), – – the model of Grosser et al. (1988), and • the experimental data of Dodds and Srivastava (2006). Details of the packing – average particle size [μm] / bed porosity: a) 370/0.3547, b) 370/0.3926, c) 254/0.3519, d) 254/0.3952, e) 188/0.3445, f) 188/0.3839, g) 117/0.3504, h) 117/0.3967.

In the measurements of Dodds and Srivastava (2006), the capillary pressure exhibited a jump at approximately $S_L \sim 0.1$. Beyond that point, no more liquid could be removed from the system even though the capillary pressure was increased. According to the current model, however, liquid saturation should continue to decrease steadily. Dodds and Srivastava (2006) used smooth glass spheres in their experiments, and thus the jump in the experimental data could be caused by a loss of hydrodynamic continuity [IV]. The assumption is supported by the experiments of Dullien et al. (1989) and Bico et al. (2002), where it has been found that surface roughness improves liquid spreading and hydrodynamic continuity. Figure 13 presents the experimental results of Dullien et al. (1988), who carried out experiments with both rough and smooth glass spheres. Here too, the capillary pressure measured with smooth particles exhibits a sudden jump at approximately $S_L = 0.1$. However, with rough particles liquid saturations close to zero could be reached and the modeled capillary pressure is well in agreement with the experimental results. Thus it was concluded that hydrodynamic continuity plays a significant role in capillary pressure measurement with smooth particles. Since nonporous, smooth catalyst materials are rarely encountered in industrial applications, the model performance with rough particles is the most relevant.

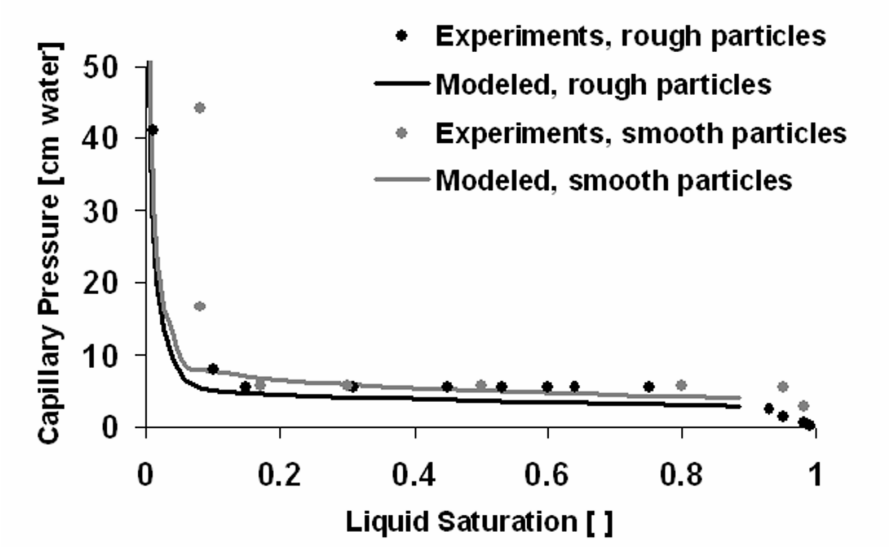

Figure 13. Comparison of the current model against the experimental data of Dullien et al. (1989) – etched (rough) and smooth glass spheres. Porosity is estimated to be 0.4.

5.2.1.1 Mixtures of particles

In addition to the measurements with uniform particle sizes, Dodds and Srivastava (2006) performed measurements with beds packed with mixtures of three different particle sizes. The extendibility of the capillary pressure to mixtures was investigated based on those measurements. Portion of the results is presented in Figure 14. The results are presented as a whole in paper [IV]. It was found that although the model was developed for uniform particle size, it can also be used in the case of mixtures of particles. This, however, requires an adjusted model for the sequential particle size.

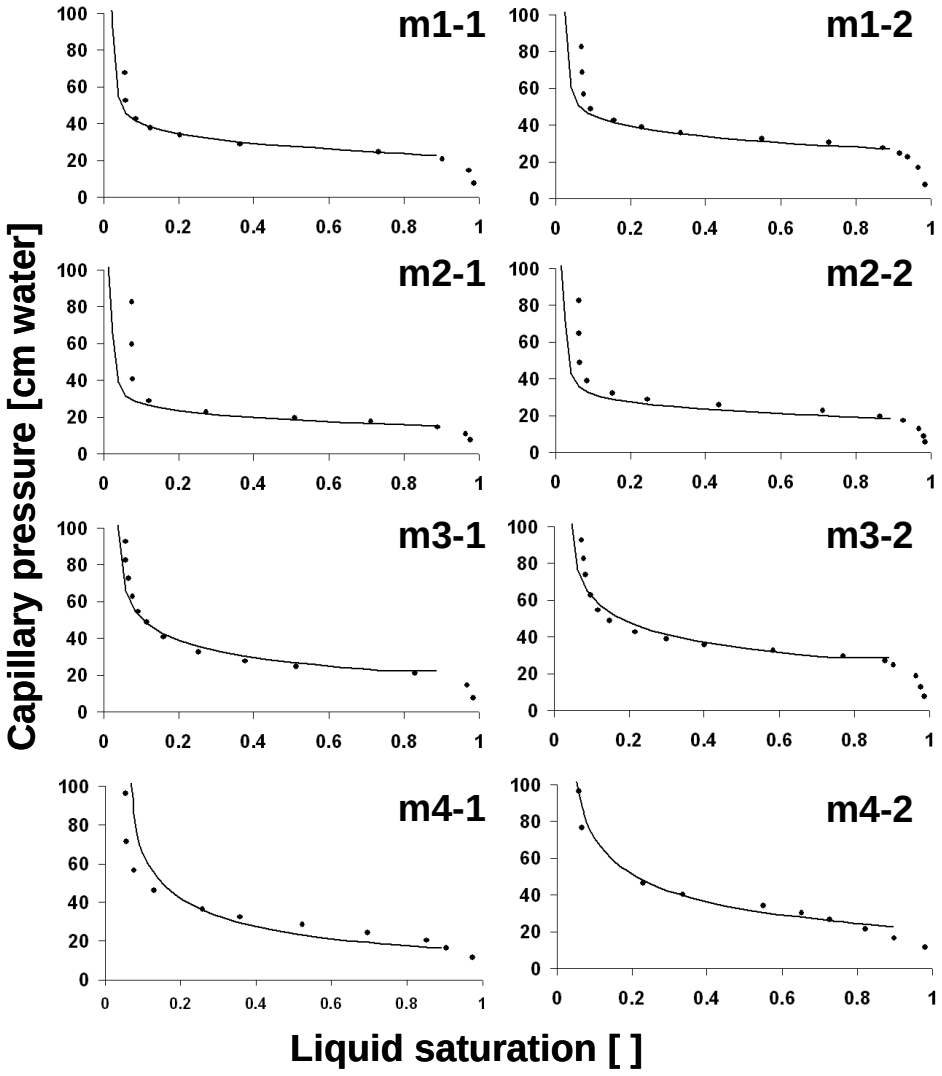

Figure 14. Comparison between the modeled and measured capillary pressures in beds packed with mixtures m1 through m4. — the new model, • the experimental data Dodds et al. (2006) with beds packed with mixtures (Dodds and Srivastava 2006). Details of the packing – D_{max}/D_{min} [μm] / bed porosity: m1-1) 170/90 / 0.392, m1-2) 170/90 / 0.354, m2-1) 258/128 / 0.388, m2-2) 258/128 / 0.343, m3-1) 187/46 / 0.390, m3-2) 187/46 / 0.332, m4-1) 258/58 / 0.340, m4-2) 258/58 / 0.303

6. CFD MODELING SETUP

Simulations were performed using a three-phase Eulerian model with a pressure based, double-precision, unsteady state solver. Laminar flow was assumed. Second and first order discretization schemes were used for the momentum and phase fractions, respectively.

6.1 Simulated cases

The simulations corresponded to the experiments presented in Boyer et al. (2005), Herskowitz and Smith (1978), and Porter et al (1968). Simulations of our own measurements were also performed [VI]. Information on the simulations is presented in Table 8 and in papers [VI] and [V].

Table 8. Details of the CFD simulations performed in papers [VI] and [V]. Unless otherwise noted, the parameters are obtained from the reference in question.

	Herskowitz and Smith (1978)	**Boyer et al. (2005)**	**Ravindra et al. (1997)**	**Paper [VI]**
Experimental setup	Cylindrical	Cylindrical	Rectangular	Rectangular
Dimensions, mm	ø 114	ø 400	80x60	250x50
Packing height (*z*), cm	55	180	20	25
Water feed system	Single point source, ø 5.4 mm	Single point source, ø 8 mm	Single point source ø 4.0 mm Line feed source	Line feed source
Superficial flow rate for water, cm/s	0.25	0.03	0.1	0.02/0.53
Superficial flow rate for air, cm/s	1.0	9.95	4.27	8.1/23.0
Packing type and size [mm]	Ceramic spheres ø 9.53/6.35/2*	Glass spheres ø 1.99	Porous alumina particles ø 1.9	Glass spheres ø 3.9
Porosity	0.4	$\varepsilon(z) = 0.421 - 0.124z + 0.047z^2$	0.39**	0.36
Spread factor***, cm	0.15/0.12/0.07	0.07	0.07	0.09
Presented in paper	[V]	[V]	[V]	[VI]

* ø 2 mm particles are included for comparison, no experimental data available

** Estimated according to Bey and Eigenbergen (1997) based on equiareal cylinder

*** Spread factors are estimated based on Baldi and Specchia (1976)

6.2 Porosity

The porosity generation for a CFD grid:

1 The mean porosity of the packing is used for bulk porosity
2 A radial porosity profile can be used to account for the higher porosities at the wall
3 A normal distribution, with a specified standard deviation, can be used to generate random variation of porosity

Of the above only the mean porosity of the packing is always required. The necessity of the other two constraints depends on the conditions and is discussed below.

6.2.1 Radial porosity profiles

The porosity near the wall of a packed bed is often higher than the bulk porosity. A radial porosity profile describes this effect. The significance of the wall effect decreases as the column to particle diameter ratio increases, making the proportion of the wall region smaller. Values from 12 to 25 have been suggested as a minimum for the column to particle diameter ratio, D_c/d_p, for uniform flow (Al-Dahhan and Duduković 1994; Baker et al. 1935; Herskowitz and Smith 1978; Porter et al. 1968; Porter and Templeman 1968; Prchlik et al. 1975). Radial porosity profiles for spheres have been proposed by several authors and are presented in Table 9. The effect of the radial porosity profile on the simulation results was tested in paper [V]. The experiments of Porter et al. (1968) were used with a column to particle ratio of only 12. It was found that the radial porosity profile had a significant effect on the simulation results. Based on the comparison, the model of Mueller et al. (1991) was found to characterize the packing structure best. It is, however, to be emphasized that the effect of the radial porosity profile on simulations is only significant when simulations are compared to laboratory experiments with a low column-to-particle diameter ratio.

6.2.2 Variation of porosity

Sometimes the random nature of porous media has been taken into account by a porosity density function (Gunjal et al. 2005; Gunjal and Ranade 2007; Jiang et al. 2002) − the local porosities are determined randomly based on a normal distribution with a specific standard deviation. In CFD the variation of porosity should depend on the cell size − the standard deviation of porosity should approach zero as the cell size grows and increase as the cell size decreases. It is important to note that the standard deviation used here differs from that used in the capillary pressure model. The capillary pressure is a property of a specific porous medium and it should not be affected by the simulation grid.

Based on the experiments (see 3.2), it was found that it is not appropriate to link the random variation of porosity to the cell volume. Instead, it is linked to the smallest cell dimension. This approach should be valid as long as the cells are likely to contain both solid and void spaces. If the cell size decreases to the point where the majority of the cells are likely to be completely solid or void, the approach is no longer valid.

The effect of random porosity on CFD simulations was examined in paper [V]. When the dispersion forces were neglected, the random variation of porosity spread the liquid to

Table 9. Literature correlations for radial porosity profiles for spheres in a cylindrical column.

Author	Radial porosity model
Bey and Eigenbergen (1997)	$x_{\min} = 0.5\left(D_c - \sqrt{\left(D_c - d_p\right)^2 - d_p^2} \right)$ $r' = \frac{1}{x_{\min}}\left(\frac{D_c}{2} - r \right) - 1$ $\varepsilon_{wall} = \varepsilon_{\min} + \left(1 - \varepsilon_{\min}\right)\left(r'\right)^2 \text{ for } r' < 0$ $\varepsilon_{core} = \varepsilon_b + \left(\varepsilon_{\min} - \varepsilon_b\right)\exp\left(-\frac{r'}{c} \right)\cos\left(\frac{\pi}{b} r' \right) \text{ for } r' \geq 0$ with $\varepsilon_{\min} = 0.24$ $b = 0.876$ $c = 10$
Cohen and Metzner (1981)	$\frac{1-\varepsilon}{1-\varepsilon_b} = 4.5\left(r^* - \frac{7}{9} r^{*2} \right), \quad r^* \leq 0.25$ $\frac{\varepsilon - \varepsilon_b}{1-\varepsilon_b} = a_1 e^{-a_2 r^*} \cos\left(a_3 r^* - a_4\right)\pi, \quad 0.25 < r^* < 8$ $\varepsilon = \varepsilon_b, \quad 8 \leq r^* < \infty$ $r^* = \left(D_c/2 - r\right)/d_p, \text{ for } 0 \leq r^*$ with a_1=0.3463; a_2=0.4273; a_3=2.4509; a_4=2.2011
Mueller (1991)	$\varepsilon = \varepsilon_b + \left(1 - \varepsilon_b\right) J_0\left(ar^*\right) e^{-br^*} \text{ for } 2.61 \leq D_c/d_p$ $a = 8.243 - \frac{12.98}{\left(D_c/d_p + 3.156\right)}, \text{ for } 2.61 \leq D_c/d_p \leq 13.0$ $a = 7.383 - \frac{2.932}{\left(D_c/d_p - 9.864\right)}, \text{ for } 13.0 < D_c/d_p$ $b = 0.304 - \frac{0.724}{D_c/d_p}$ $r^* = \left(D_c/2 - r\right)/d_p, \text{ for } 0 \leq r^*$
Sun et al. (2000)	$\varepsilon = 1 - \left(1 - \bar{\varepsilon}\right)\left\{ 1 - \exp\left(-2\left(\frac{D_c/2 - r}{d_p} \right)^2 \right) \right\}$

some extent. This is because it affects the local phase interaction forces. However, when dispersion forces were included, the random variation of porosity did not have a significant effect on overall liquid spreading. Therefore variation of porosity can be seen as an unsuitable way to compensate the lack of proper dispersion forces. When dispersion forces are included, variation of porosity merely adds some random noise to the simulation results, which may unnecessarily complicate comparisons between experiments.

6.3 Parameters for the mechanical dispersion model

The only estimated parameter for the mechanical dispersion model is the spread factor *S*. The number of literature correlations available for spread factors is scarce. Table 10 lists three of these correlations.

Since molecular diffusion cannot be neglected in all dispersion experiments, resulst are not always reported as spread factors, but instead as transverse dispersion coefficients, D_T, which also includes the effect of molecular diffusion. The spread factor and dispersion coefficient are related to one another by a simple expression (Bear 1979; Hoek et al. 1986; Potucek 1997; Sahimi et al. 1986a):

$$D_T = S\left|u_{\|}\right| \tag{55}$$

By neglecting the effect of molecular dispersion (i.e. $D_m = 0$) and applying equation (55) the following equation is obtained. $Pe_T(\infty)$ refers to an asymptotic value of the transverse Péclet number, Pe_T, as the Reynolds number approaches infinity (Coelho and Guedes de Carvalho 1988; Guedes de Carvalho and Delgado 2005; Gunn 1987):

$$\frac{1}{Pe_{mech}} = \frac{1}{\tau}\frac{1}{Pe_m} + \frac{1}{Pe_{mech}(\infty)} \xrightarrow{D_m=0} D_{mech} = \frac{d_p}{Pe_{mech}(\infty)}\left|u_{\|}\right| \rightarrow S = \frac{d_p}{Pe_{mech}(\infty)} \tag{56}$$

The spread factor correlations (Table 10) and equation (56) were analyzed in paper [V], on the basis of which the model of Baldi and Specchia (1976) was found to be the most coherent with the experimental data (Cihla and Smith 1958; Kolomaznik et al. 1971; Porter et al. 1968).

Table 10. Literature models for spread factors.

Author	Correlation	Particles used in the experiments
Baldi and Specchia (1976)	$S[m] = 0.015\left(\frac{d_p}{m}\right)^{0.5}\varphi_{eff}^{-1/3\,*}$	Raschig rings, Berl saddles
Hoek et al. (1986)	$S = 0.12 d_p$	Raschig rings, Intalox saddles
Onda et al. (1973)	$S[m] = 0.231\left(\frac{d_p}{m}\right)^{0.5}\left(\frac{\sigma}{N/m}\right)$	Beads, Berl saddles, Raschig rings

* The constant value was corrected based on Figure 7 in Baldi and Specchia (1976)

6.4 Parameters for the capillary pressure model

In the capillary pressure model, the following parameters are required: mean particle size, particle size range, liquid-solid contact angle, mean porosity and the standard deviation of porosity. In the simulations presented in papers [V] and [VI], most of the above parameters were known, but the contact angle and the standard deviation of porosity had to be estimated. The standard deviation of porosity was estimated based on the correlation proposed in paper [IV]:

$$\sigma_\varepsilon = 0.2621\bar{\varepsilon} - 0.068 \tag{57}$$

Several literature values for the air-water-glass contact angle have been reported (e.g. Gunjal et al. 2003b; Laroussi and De-Backer 1979; Lin et al. 1996; Moseley and Dhir 1996) with a great deal of discrepancy among them. The value 29° that was reported by Moseley and Dhir (1996) is used here since their measurement method and conditions are the closest to the flow conditions in trickle-bed reactors. They used a single sphere and determined the receding air-water-glass contact angle by drawing liquid away from the initially wetted sphere.

Since Herskowitz and Smith (1978) did not report the detailed material information on the ceramic spheres used in their experiments, the air-water-ceramic contact angle is not known. The contact angle is based on the measurements of Oh et al. (2002), who measured contact angles between multiple ceramic surfaces and water. The measured receding air-water-ceramic contact angles were between 4.5° and 44.9°, depending on the ceramic type and surface roughness. The air-water-glass contact angle of 29° is close to the average of the values measured by Oh et al. (2002) and is thus used also for the air-water-ceramics contact angle.

For the porous alumina particles used by Ravindra et al (1997), a contact angle of zero was used due to the porous nature of the material.

7. LIQUID DISPERSION SIMULATIONS WITH CFD

CFD simulations were performed to test the ability of the current model to predict liquid dispersion. The simulated cases were selected based on the following criteria: 1) spherical particles were used in the experiments due to the assumptions behind the capillary pressure model, 2) the experimental setup was reported in detail to provide all the necessary data for the simulations and 3) the experimental results were reported so that they could be used for comparison. In all the simulations presented below, the capillary and mechanical dispersion models are both included. A general summary of the simulated cases is presented in Table 8.

7.1 PRE-STUDY: SIGNIFICANCE OF DISPERSIVE FORCES

In CFD, all added source terms complicate the solution, which means that shorter time steps and more iterations are required. Since overloading (i.e. spreading of the liquid on top of the bed) is caused by the phase interaction forces, it cannot be discarded from simulations, but either capillary or mechanical dispersion could be, if found to be insignificant. From Table 3 it can be seen that particle size has an opposite effect on capillary and mechanical dispersion – an increase in particle size increases mechanical and decreases capillary dispersion and vice versa. Therefore in paper [V], it was investigated whether either capillary or mechanical dispersion could be omitted in the particle size range used in industrial trickle-bed reactors. The simulation grid corresponded to the experimental setup of Herskowitz and Smith (1978) and the particle sizes used in the simulations were ø 2.00 mm, ø 6.35 mm, and ø 9.53 mm spheres.

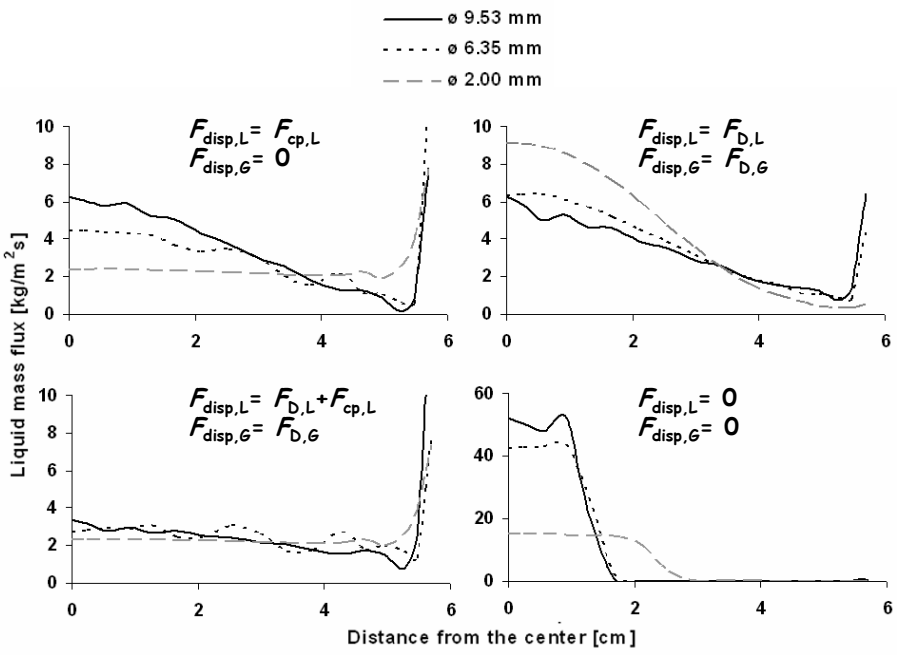

Figure 15. Significance of the capillary and mechanical dispersive forces in the overall liquid dispersion in the case of ø 2 mm, ø 6.35 mm, and ø 9.53 mm spherical particles.

It was found that, within the particle size range used, neither of the dispersion mechanisms became insignificant [V]. Figure 15 presents the simulation results. Since overloading increases as the particle size decreases, it has to be considered when evaluating the importance of dispersion mechanisms. Based on Figure 15 it was concluded that with a mean porosity of 0.4, mechanical and capillary dispersion are approximately equally significant for ø 9.53 mm spheres. For ø 2.00 mm spheres, capillary dispersion already starts to dominate over mechanical dispersion, but the mechanical dispersion is still not insignificant. Since the porosity affects the capillary pressure, changes in porosity also affect the relation between capillary and mechanical dispersion. Nevertheless, it seems that both dispersion mechanisms should be considered with the industrially relevant particle sizes, which range approximately from 1 to 4 mm (Westerterp and Wammes 2005).

7.2 Experiments of Herskowitz and Smith (1978)

Herskowitz and Smith (1978) measured liquid dispersion in a cylindrical column with ø 9.53 mm and ø 6.35 mm spheres. The liquid dispersion was measured with a collector device, which consisted of four sectors having outer diameters of 5.09, 7.66, 9.90, and 11.61 cm. The outer diameter of the outermost collector was slightly larger than the column diameter to prevent leakage. The simulations are presented in detail in paper [VI]. The simulated liquid mass fluxes along the bed length are presented in Figure 16. The results are compared to the measurements of Herskowitz and Smith (1978) at three different bed heights in Figure 17. The simulated liquid flow profiles are in excellent agreement with the measurements at all bed heights.

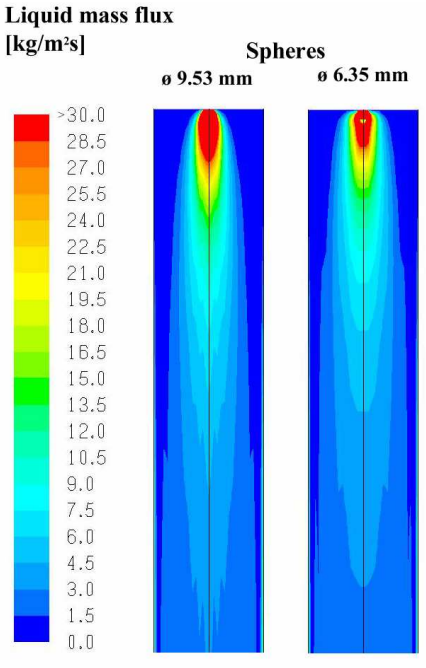

Figure 16. Simulated liquid mass fluxes along the reactor length for ø 9.53 mm (left) and ø 6.35 mm (right) spheres.

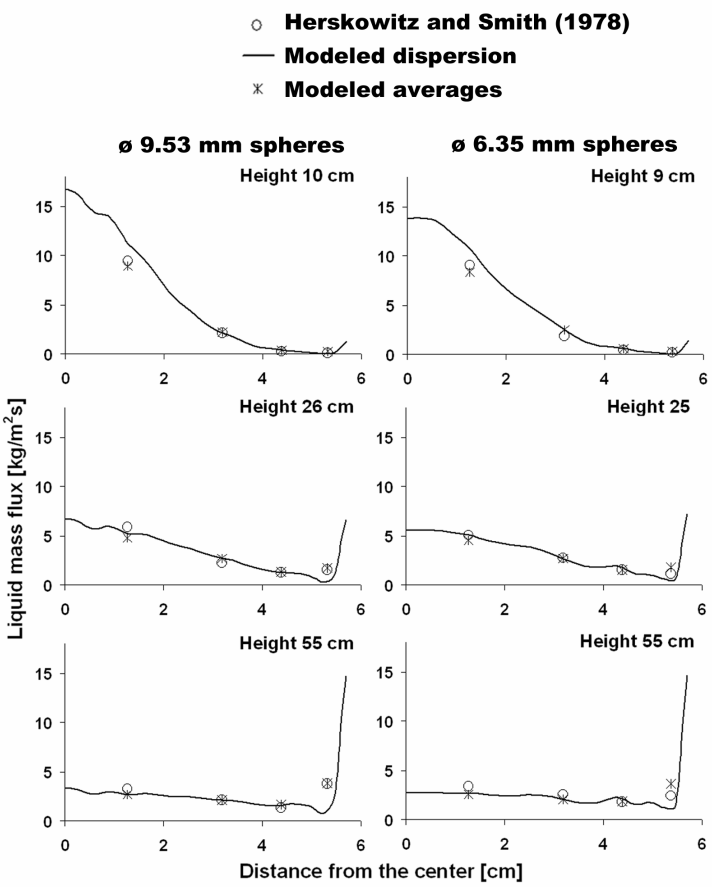

Figure 17. Comparison of the simulated dispersion profiles to the experimental results of Herskowitz and Smith (1978). Modeled averages are the average mass fluxes through the four collector sectors of the collector grid used in the measurements.

7.3 Experiments of Boyer et al. (2005)

Boyer et al. (2005) measured liquid saturation profiles using gamma-ray tomography for ø 1.99 mm glass spheres. The measurements were performed in a 1.8 m high column with gamma-ray tomography at 60 mm and 280 mm below the feed point. The simulation results reproduced the measured liquid saturation well when the distance from the center was more than approximately 3−4 cm and succeeded in predicting the overall spread angle of the liquid jet correctly [V]. At the center of the column the measured liquid saturations were somewhat unusual when compared to the experimental data obtained with liquid collector systems (Herskowitz and Smith 1978; Porter et al. 1968; Prchlík et al. 1975; Saroha et al. 1998). One possible explanation is that the reconstruction algorithm in the tomographic measurements underpredicts the liquid saturations near the column center. If the anomalous region (0 – 3 cm from the center), which is less than 2.3 % of the total column surface area, is neglected, the performance of the model is very good, as demonstrated in Figure 18.

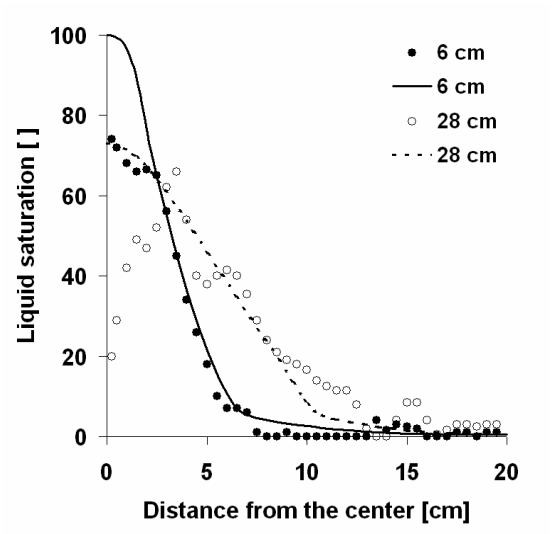

Figure 18. Comparison of the simulated liquid saturation profiles to the measurements of Boyer et al. (2005).

7.4 Experiments of Ravindra et al. (1997)

Ravindra et al. (1997) performed point and line liquid feed experiments with ø 1.9 mm porous alumina particles in a rectangular column. Since the column was not symmetric the simulations were performed in a three-dimensional grid that corresponded to a quarter of the experimental setup. The results are presented in Figure 19 and Figure 20 for the line and point source feeds, respectively. The simulated liquid dispersions correspond well with experimental data; especially in the case of the line feed system. In the case of the point feed system, there is a peculiar feature in the experiments: the liquid spreading along the shorter side was less than along the longer side of the column. This phenomenon results most probably from the structure of the experimental bed and, without more information, cannot be reproduced by simulations. Thus, on average, the results are considered to be good.

7.5 Experiments from paper [VI]

The experimental setup presented in Figure 2 was simulated in paper [VI]. Simulations were performed for three different cases that varied in gas and/or liquid flow rates. In all cases the simulated flow profiles agreed satisfactorily with the experiments. The largest difference was in case 1, where the liquid flow rate was particularly small – only 0.02 cm/s (Figure 21). Measurements with such a low liquid flow rate were performed to prevent overloading. The experiment was, however, very susceptible to measurement errors; the significance of flow abnormalities, such as strayed rivulets, was overemphasized as even small rivulets constitute a fairly large percentage of the total flow. The best agreement can be found in case 3, where the gas and liquid flow rates are the largest. The effect of an increased gas flow rate is reproduced in the simulations, although it is smaller than in the measurements.

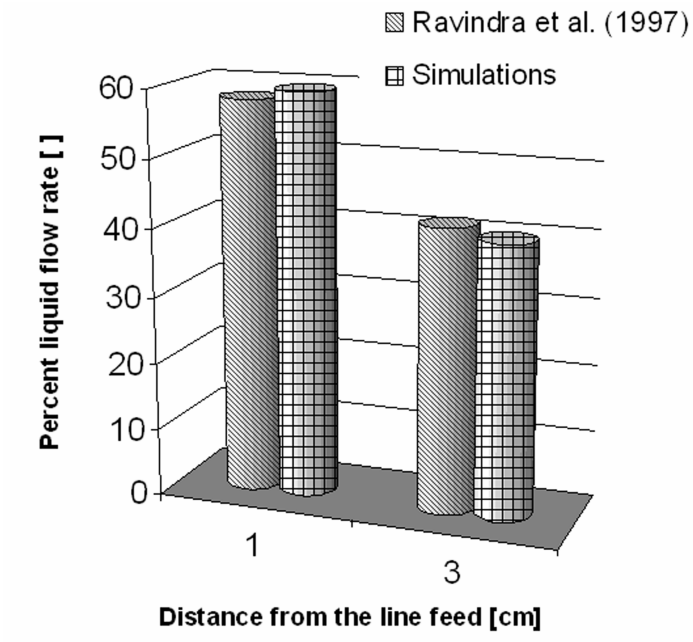

Figure 19. Comparison of the simulated liquid saturation profiles to the measurements of Ravindra et al. (1997); line source feed of liquid.

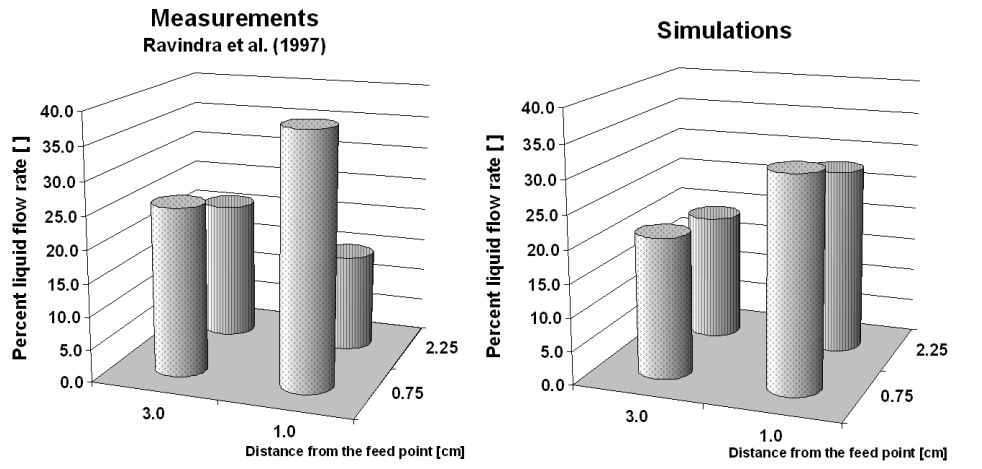

Figure 20. Comparison of the simulated liquid saturation profiles to the measurements of Ravindra et al. (1997); point source feed of liquid.

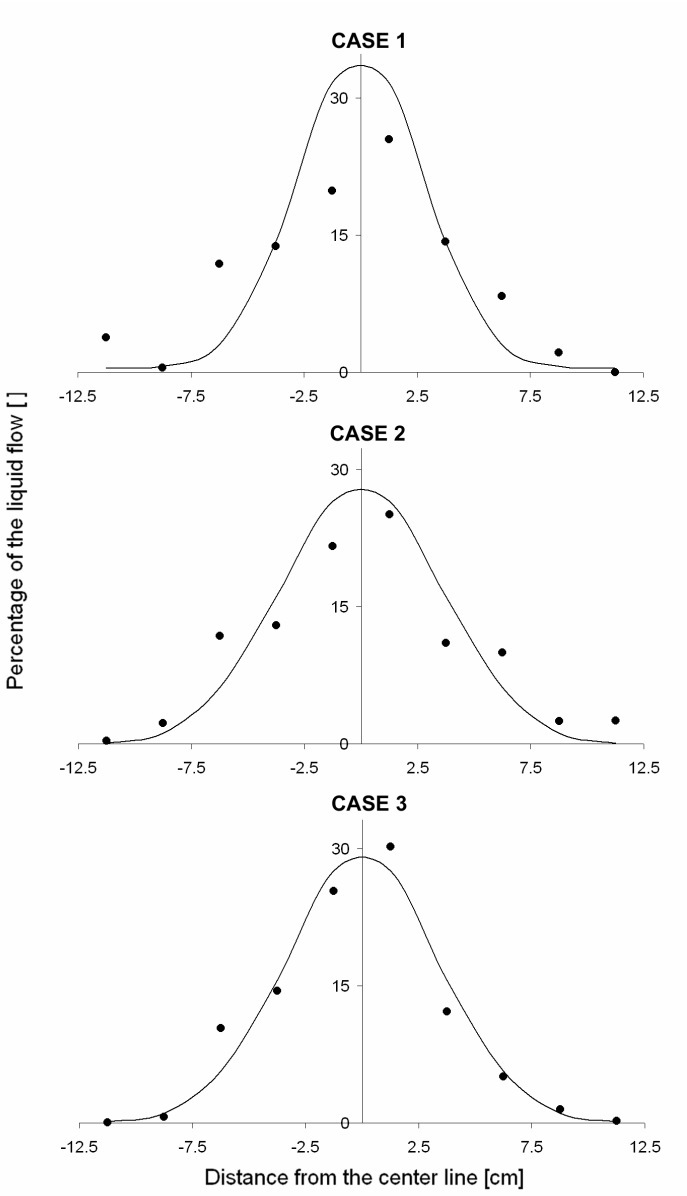

Figure 21. Comparison of the simulated and measured flow profiles. Case 1: U_L = 0.02 cm/s, U_G = 8.1 cm/s; Case 2: U_L = 0.53 cm/s, U_G = 8.1 cm/s; Case 3: U_L = 0.53 cm/s, U_G = 23.0 cm/s.

8. CONCLUSION

A new hydrodynamic model for trickle-bed reactors has been developed. The model includes phase interaction models that can be used to solve a two-phase pressure drop and liquid holdup in uniform flow conditions. The model parameters were fitted against a vast experimental database. The model also accounts for the partial wetting of the catalyst and provides an estimation of the liquid-solid wetting efficiency. [III]

It was shown that for a non-uniform flow, the gas-liquid-solid phase interactions alone are no longer sufficient to describe the hydrodynamics in trickle-bed reactors; liquid dispersion also has to be accounted for [V], [VI]. The phase interactions alone account only for liquid spreading due to overloading. Overloading signifies the spreading of liquid at the top of the packing due to a local peak in the pressure drop, caused for example by a local liquid feed source. In addition to overloading, spreading of liquid was attributed to capillary and mechanical dispersion.

Capillary dispersion is caused by capillary pressure gradients and thus a new capillary pressure model was developed [IV]. The model was developed based on the analytical analysis of pendular and funicular liquid structures at the interstices of spherical particles, thus limiting the model for spheres. When compared to the capillary pressure models previously used in trickle-bed reactor modeling, the new model showed improvement especially in the pendular regime. This is important, since capillary dispersion is most significant when liquid saturation approaches zero. The model predictions were also compared to capillary pressure measurements with non-porous and porous spheres. In the case of smooth, non-porous particles, it was observed that the measured capillary pressure exhibited a sudden rise, which was not reproduced by the model. It was suspected that the sudden rise was caused by the breakage of the liquid film. If the hydrodynamic continuity is lost, liquid cannot exit the bed even if the capillary pressure increases. This conclusion was supported by the results with porous particles, where a sudden rise was not observed and the model reproduced the experimental results well. Since porous particles are nominally used in industrial trickle-bed applications, the performance of the model in the case of porous particles is the most important.

Mechanical dispersion in trickle-bed reactors has been previously simulated only for tracer spreading. However, there has not been a CFD model for the mechanical dispersion of gas and liquid phases. Therefore, in the course of this thesis, a model for the mechanical dispersion of liquid was presented [V]. The different characteristics of tracer and liquid dispersion were discussed from a theoretical and modeling point of view. In tracer dispersion there is no momentum transfer, but in liquid dispersion there is. This means that even if the capillary dispersion and overloading could be assumed to be insignificant, the phase interaction forces will still have an impact on liquid spreading. As a result, the simulated spreading of tracer is more than that of liquid even if the spread factor used in the model is the same. It was also questioned whether the normal distribution approach can be used in liquid dispersion for results analysis, since the assumption of a uniform liquid velocity field is not correct.

The relation between mechanical and capillary dispersion was investigated by means of CFD simulations [V]. Since every additional source term complicates the solution in CFD, it was investigated whether both of the dispersion forces were significant when

industrially relevant particle sizes were used. Although capillary dispersion was clearly the dominant dispersion source with ø 2 mm spheres, mechanical dispersion could not be considered insignificant. With ø 9.53 mm particles, capillary and mechanical dispersion were found to be approximately of equal significance. It is therefore recommended that they should both be considered. In addition, CFD simulations of several experimental cases were performed. The data included both non-porous and porous spheres. The correspondence between the experiments and simulations was found to be good.

9. FUTURE RESEARCH RECOMMENDATIONS

Although significant work has been done in an attempt to improve trickle-bed reactor flow modeling, there are still some unanswered questions that should be addressed in future research, as well as goals for future model development. In this thesis, the discrepancies between mechanical dispersion of tracer and liquid have been touched upon, but they are still not thoroughly understood. This should be examined further and the effect on experiment and CFD simulations should also be considered.

Due to the restrictions of the current capillary pressure model, all cases simulated in this thesis were beds packed with spheres. The industrially relevant particle shapes are, however, in most cases non-spherical, which raises the need for the further development of the capillary pressure model. The capillary pressure for spheres was developed based on analytical reasoning, but for non-spherical particles the analytical analysis of the packing structure is not possible. Thus different ideas on how the capillary pressure model could be extended for non-spherical particles based on laboratory experiments and CFD simulations should be elaborated.

Although the model has successfully captured the flow fields in non-uniform flow situations, there are still some questions concerning the liquid holdup and pressure drop in such conditions. In uniform, or close to uniform flow conditions, the model performs quite well in predicting pressure drop and liquid holdup. In non-uniform flow conditions, however, the pressure drop is often under-predicted and the static holdup of liquid is quite small – at least with nonporous particles. A similar issue was also encountered in the development of the capillary pressure model. It was then concluded that the high liquid saturations in the experiments are probably caused by the breakage of the liquid film and the consequent loss of hydrodynamic continuity. This is not accounted for in the model. It is common with nonporous, smooth particles, but not as severe with the porous particles that are commonly used in industrial trickle beds. A similar explanation could lie behind the low static holdups encountered in the simulations, which would also cause the under-prediction of pressure drop due to the too high effective porosity encountered by the gas phase. In future work, this issue should be addressed and the theory about lost hydrodynamic continuity should be tested based on simulations with porous particles.

NOTATION

a_t	Packing external surface area per unit volume of reactor, [m^{-1}]
A, B	Parameters in equation (13)
A_c	Cross-sectional are, [m^2]
$B(X)$	Bias, equation (51)
d_p	Particle diameter, [m]
D	Coefficient of diffusion, [$m^{2}\cdot s^{-1}$]
D_c	Column diameter, [m]
D_H	Hydraulic diameter, [m]
D_m	Coefficient of molecular diffusion, [$m^{2}\cdot s^{-1}$]
D_{mech}	Coefficient of mechanical dispersion, [$m^{2}\cdot s^{-1}$]
$\langle e_X \rangle$	Mean relative error as defined in equation (50)
E_μ, E_ρ	One-phase-specific Ergun coefficients, [ ]
$E_{\mu,k}, E_{\rho,k}$	Phase-specific Ergun coefficients for phase *k*
f_e	Wetting efficiency
f_τ	Friction factor
$f(\varepsilon)$	Probability density function of beta distribution
$F_{cp,L}$	Capillary dispersion force for liquid, [$N\cdot m^{-3}$]
$F_{D_i,k}$	Component *i* of the mechanical dispersion force vector for phase *k*, [$N\cdot m^{-3}$]
$F_{\mathrm{disp},k}$	Total dispersive force for phase *k*, [$N\cdot m^{-3}$]
$F_{\mathrm{int},k}$	Total interaction force for phase *k*, [$N\cdot m^{-3}$]
F_{kj}	Phase interaction force between phases *k* and *j*, [$N\cdot m^{-3}$]
g	Gravitational acceleration constant, [$m\cdot s^{-2}$]
$J_0(x)$	Bessel J-function
k_i	Adjustable parameters in equations (40) – (42)
K_{kj}	Coefficient of interaction force between phases *k* and *j*, [$N\cdot s\cdot m^{-4}$]
L	Sample size in equation (1), [cm]
L_m	Liquid superficial mass velocity, [$kg\cdot m^{-2}\cdot s^{-1}$]
N_c	Number of particle-particle contact points per particle
p	Pressure, [Pa]
p_c	Capillary pressure, [Pa]
p', q'	Parameters in equation (33)
$\Delta P / \Delta L$	Pressure drop, [$Pa\cdot m^{-1}$]
r	Radial coordinate, [m]
r_1, r_2	$r_i = R_i / R, \quad i = 1,2$
R	Particle radius, [m]
R_1, R_2	Two principal radii of a pendular ring, [m]
R^*	Local curvature of the interface, [m]

s	Length of the wetted perimeter, [m]
S	Spread factor, [m]
S_L	Liquid saturation
STD_e	Standard deviation of the relative error around the mean relative error, equation (52)
t	Time, [s]
T_0	Empty bed tortuosity
T_k	Phase-specific tortuosity of phase *k*
$u_{D_i,k}$	Component *i* of the drift velocity vector for phase *k*, [m·s^{-1}]
u'_G	Modified gas velocity, [m·s^{-1}]
u_k	Interstitial velocity of phase *k*, [m·s^{-1}]
U_k	Superficial velocity of phase *k*, [m·s^{-1}]
V	Volume, [m^3]
X	$X = (1-\cos\varphi)$
$Y_{i,L}$	Mass fraction of component *i* in the bulk liquid phase

Greek letters

α	Gas saturation
ε	Porosity in the packed bed
$\bar{\varepsilon}$	Mean porosity of the packed bed
ε_b	Bulk porosity of the packing
φ	Filling angle, [rad]
φ_{eff}	Sphericity
$\Gamma(x)$	Gamma function
μ_k	Viscosity of phase *k*, [Pa·s]
θ	Gas-liquid-solid contact angle, [rad]
θ_k	Volume fraction of phase *k*
ρ_k	Density of phase *k*, [m^3·kg^{-1}]
σ	Gas-liquid-solid surface tension, [N·m^{-1}]
σ_ε	Standard deviation of porosity
τ	Tortuosity

Dimensionless groups

Eö′	Modified Eötvös number, $\text{Eö}' = \rho_L g d_p^2 \varepsilon^2 / \left[\sigma(1-\varepsilon)^2\right]$
Fr_G	Gas Froude number, $\text{Fr}_G = U_G / \sqrt{g d_p}$
Fr_L^*	Modified liquid Froude number, $\text{Fr}_L^* = a_t L_m^2 / \rho_L^2 g$
Ga_k	Galileo number for phase *k*, $\text{Ga}_k = \rho_k^2 g d_p^3 / \mu_k^2$
Ga'_k	Packed-bed Galileo number for phase *k*, $\text{Ga}'_k = \rho_k^2 g d_p^3 \varepsilon^3 / \left[\mu_k^2 (1-\varepsilon)^3\right]$
Pe_m	Péclet number based on molecular dispersion coefficient, $\text{Pe}_m = u d_p / D_m$

Pe_{mech}	Péclet number based on transverse dispersion coefficient, $\mathrm{Pe}_{mech} = ud_p / D_{mech}$
Re_k	Reynolds number for phase *k*, $\mathrm{Re}_k = \rho_k d_p U_k / \mu_k$
Re'_k	Packed-bed Reynolds number for phase *k*, $\mathrm{Re}'_k = \rho_k d_p U_k / (\mu_k (1-\varepsilon))$
We^*_L	Modified liquid Weber number, $\mathrm{We}^*_L = L_m^2 / \sigma \rho_L a_t$

Subscripts

G	Gas
f	Fluid in a pendular ring
fcc	Face-centered cubic packing
fun	Funicular
L	Liquid
LF	Liquid-full
nw	Non-wetting phase
pend	Pendular
R	Reactor
sc	Simple cubic packing
seq	Sequential variable
tr	Value at the pendular-funicular transition point
TP	Two-phase
w	Wetting phase

REFERENCES

Al-Dahhan, M.H., Duduković, M.P., 1994. Pressure drop and liquid holdup in high pressure trickle bed reactors. Chemical Engineering Science, 49, 5681–5698.

Al-Dahhan, M.H., Duduković, M.P., 1995. Catalyst wetting efficiency in trickle-bed reactors at high pressure. Chemical Engineering Science, 50, 2377−2389.

Al-Dahhan, M.H., Khadilkar, M.R., Wu, Y., Duduković, M.P., 1998. Prediction of pressure drop and liquid holdup in high-pressure trickle-bed reactors. Industrial & Engineering Chemistry Research, 37, 793−798.

Alicilar, A., Bıçer, A., Murathan, A., 1994. The relation between wetting efficiency and liquid holdup in packed columns. Chemical Engineering Communications, 128, 95−107.

Atta, A., Roy, S., Nigam, D.P., 2007. Investigation of liquid maldistribution in trickle-bed reactors using porous media concept in CFD. Chemical Engineering Science, 62, 7033–7044.

Attou, A., Boyer, C., Ferschneider, G., 1999. Modelling of the hydrodynamics of the cocurrent gas-liquid trickle flow through trickle-bed reactor. Chemical Engineering Science, 54, 785−802.

Attou, A., Ferschneider, G., 2000. A two-fluid hydrodynamic model for the transition between trickle and pulse flow in a cocurrent gas-liquid packed-bed reactor. Chemical Engineering Science, 55, 491−511.

Baker, T., Chilton, T.H., Vernon, H.C., 1935. The course of liquid flow in packed towers. Transactions of the American Institute of Chemical Engineers, 31, 296–315.

Baldi, G., Specchia, V., 1976. Distribution and radial spread of liquid in packed towers with two-phase cocurrent flow: effect of packing shape and size. Quaderni dell'Ingegnere Chimico Italiano, 12, 107−111.

Barnett, V., 1975. A simple random walk on parallel axes moving at different rates. Journal of Applied Probability, 12, 466–476.

Baussaron, L., Julcour-Lebigue, C., Wilhelm, A.-M., Boyer, C., Delmas, H., 2007. Partial wetting in trickle bed reactors: measurement techniques and global wetting efficiency. Industrial & Engineering Chemistry Research, 46, 8397–8405.

Bear. J., 1979. *Hydraulics of Groundwater.* McGraw-Hill.

Benkrid, K., Rode, S., Midoux, N., 1997. Prediction of pressure drop and liquid saturation in trickle-bed reactors operated in high interaction regime. Chemical Engineering Science, 52, 4021–4032.

Bensetiti, Z., Larachi, F., Grandjean, B.P.A., Wild, G., 1997. Liquid saturation in cocurrent upflow fixed-bed reactors: a state of the art correlation. Chemical Engineering Science, 52, 4239–4247.

Bey, O., Eigenbergen, G., 1997. Fluid flow through catalyst filled tubes. Chemical Engineering Science, 52, 1365−1376.

Bico, J., Thiele, U., Quéré, D., 2002. Wetting of textured surfaces. Colloids and Surfaces, 206, 41−46.

Borkink, J.G.H., van de Watering, C.G., Westerterp, K.R., 1992. The statistical character of bed-scale effective heat transfer coefficient for packed-beds. Transactions of the Institution of Chemical Engineers, Part A, 70, 610−619.

Boyer, C., Koudil, A., Chen, P., Duduković, M.P., 2005. Study of liquid spreading from a point source in trickle bed via gamma-ray tomography and CFD simulation. Chemical Engineering Science, 60, 6279−6288.

Bradford, S.A., Leij, F.J., 1995. Wettability effects on scaling two- and three-fluid capillary pressure – saturation relations. Environmental Science & Technology, 29, 1446–1455.

Burghardt, A., Bartelmus, G., Jaroszynski, M., Kolodziej, A., 1995. Hydrodynamics and mass transfer in a three-phase fixed-bed reactor with cocurrent gas-liquid downflow. Chemical Engineering Journal, 58, 83−99.

Carman, P.C., 1959. *Flow of Gases through Porous Media*, New York: Academic Press Inc.

Cihla, Z., Schmidt, O., 1958. Studies of the behaviour of liquids when freely trickling over the packing of a cylindrical tower. Collection of Czechoslovak Chemical Communications, 23, 569−577.

Clements, L.D., Schmidt, P.C., 1980. Two-phase pressure drop in cocurrent downflow in packed beds: air-silicone oil systems. AIChE Journal, 26, 314–317.

Coelho, M.A.N., Guedes de Carvalho, J.R.F., 1988. Transverse dispersion in granular beds. Part I. Mass transfer from a wall and the dispersion coefficient in packed beds. Chemical Engineering Research and Design, 66, 165−177.

Cohen, Y., Metzner, A.B., 1981. Wall effects in laminar flow of fluids through packed beds. AIChE Journal, 27, 705–715.

Colombo, A.J., Baldi, G., Sicardi, S., 1976. Solid-liquid contacting effectiveness in trickle bed reactors. Chemical Engineering Science, 31, 1101–1108.

Dallavalle, J.M., 1948. *Micromeritics: The Technology of Fine Particles*, New York: Pitman Publishing Corporation.

Demond, A.H., Roberts, P.V., 1991. Effect of interfacial forces on two-phase capillary pressure – saturation relations. Water Resources Research, 27, 423–437.

Dodds, J.A., Srivastava, P., 2006. Capillary pressure curves of sphere packings: Correlation of experimental results and comparison with predictions from a network model of pore space. Particle & Particle Systems Characterization, 23, 29−39.

Dullien, F.A.L., Zarcone, C., Macdonald, I.F., Collins, A., Bochard, R.D.E., 1989. The effect of surface roughness on the capillary pressure curves and the heights of capillary rise in glass bead packs. Journal of Colloid and Interface Science, 127, 362−372.

Dullien, F.A.L., 1992. *Porous Media: Fluid Transport and Pore Structure*. San Diego, California: Academic Press, Inc.

El-Hisnawi, A.A., Duduković, M.P., Mills, P.L., 1982. Trickle-bed reactors: Dynamic tracer tests, reaction studies, and modeling reactor performance. ACS Symposium Series, 196, 421−440.

Ellman, M.J., Midoux, N., Laurent, A., Charpentier, J.C., 1988. A new improved pressure drop correlation for trickle-bed reactors. Chemical Engineering Science, 43, 2201−2206.

Ellman, M.J., Midoux, N., Wild, G., Laurent, A., Charpentier, J.C., 1990. A new improved liquid hold-up correlation for trickle-bed reactors. Chemical Engineering Science, 45, 1677−1684.

Fourar, M., Lenormand, R., Larachi, F., 2001. Extending the F-function concept to two-phase flow in trickle beds. Chemical Engineering Science, 56, 5987−5994.

Fu, M.-S., Tan, C.-S., 1996. Liquid holdup and axial dispersion in trickle-bed reactors. Chemical Engineering Science, 51, 5357–5361.

Gardner, W., Gardner, J.H., 1953. The liquid-vapor interface in the ideal soil. Soil Science, 76, 135−142.

German R.W., 1989. *Particle Packing Characteristics*. Princeton: Metal Powders Industries Federation.

Gladden, L.F., Lim, M.H.M., Mantle, M.D., Sederman, A.J., Stitt, E.H., 2003. MRI visualisation of two-phase flow in structured supports and trickle-bed reactors. Catalysis Today, 79–80, 203–210.

González-Mendizabal, D., Aquilera, M.E., Pironti, F., 1998. Solid-liquid mass transfer and wetting factors in trickle bed reactors: effect of the type of solid phase and the presence of chemical reaction. Chemical Engineering Communications, 169, 37–55.

Grosser, K., Carbonell, R.G., Sundaresan, S., 1988. Onset of pulsing in two-phase cocurrent downflow through a packed bed. AIChE Journal, 34, 1850−1860.

Guedes de Carvalho, J.R.F., Delgado, J.M.P.Q., 2005. Overall map and correlation of dispersion data for flow through granular packed beds. Chemical Engineering Science, 60, 365−375.

Gunjal, P.R., Ranade, V.V., Chaudhari, R.V., 2003a. Liquid distribution and RTD in trickle bed reactors: Experiments and CFD simulations. Canadian Journal of Chemical Engineering, 81, 821−830.

Gunjal, P.R., Ranade, V.V., Chaudhari, R.V., 2003b. Experimental and computational study of liquid drop over flat and spherical surfaces. Catalysis Today, 79−80, 267−273.

Gunjal, P.R., Kashid, M.N., Ranade, V.V., Chaudhari, R.V., 2005. Hydrodynamics of trickle-bed reactors: experiments and CFD modeling. Industrial & Engineering Chemistry Research, 44, 6278−6294.

Gunjal, P.R., Ranade, V.V., 2007. Modeling of laboratory and commercial scale hydro-processing reactors using CFD. Chemical Engineering Science, 62, 5512−5526.

Gunn, D.J., 1987. Axial and radial dispersion in fixed beds. Chemical Engineering Science, 42, 363−373.

Gvirtzman, H., Roberts, P.V., 1991. Pore space spatial analysis of two immiscible fluids in porous media. Water Resources Research, 27, 1165−1176.

Haughey, D.P., Beveridge, G.S.G., 1966. Local voidage variation in a randomly packed bed of equal-sized spheres. Chemical Engineering Science, 21, 905−916.

Herskowitz M., Smith, J.M., 1978. Liquid distribution in trickle-bed reactors. AIChE Journal, 24, 739−454.

Herskowitz, M., Carbonell, R.G., Smith, J.M., 1979. Effectiveness factors and mass transfer in trickle-bed reactors. AIChE Journal, 25, 272−283.

Herskowitz, M., 1981. Wetting efficiency in trickle-bed reactors: its effect on the reactor performance. *Chemical Engineering Journal*, 22, 167−175.

Herskowitz, M., Smith, J.M., 1983. Trickle-bed reactors: A review. AIChE Journal, 29, 1−18.

Hoek, P.J., Wesselingh, J.A., Zuiderweg, F.J., 1986. Small scale and large scale liquid maldistribution in packed columns. Chemical Engineering Research and Design, 64, 431−449.

Holub, R.A., 1990. *Hydrodynamics of Trickle Bed Reactors*. St. Louis, MO: Washington University, D.Sc. thesis.

Holub, R.A., Duduković, M.P., Ramachandran, P.A., 1992. Phenomenological model for pressure drop, liquid holdup, and flow regime transition in gas liquid trickle flow. Chemical Engineering Science, 47, 2343-2348.

Holub, R.A., Duduković, M.P., Ramachandran, P.A., 1993. Pressure drop, liquid holdup, and flow regime transition in trickle flow. AIChE Journal, 39, 302−321.

van Houwelingen, A.J., 2006. *The morphology of solid-liquid contacting efficiency in trickle-flow*. Pretoria, South-Africa: University of Pretoria, M.Sc. thesis.

van Houwelingen, A.J., Sandrock, C., Nicol, W., 2006. Particle Wetting Distribution in Trickle-Bed Reactors. AIChE Journal, 52, 3532–3542.

Iliuta, I., Thyrion, F.C., Muntean, O., 1996. Hydrodynamic characteristics of two-phase flow through fixed beds: air/Newtonian and non-Newtonian liquids. Chemical Engineering Science, 51, 4987–4995.

Iliuta, I., Thyrion, F.C., 1997. Flow regimes, liquid holdups and two-phase pressure drop for two-phase cocurrent downflow and upflow through packed beds: air/Newtonian and non-Newtonian liquid systems. Chemical Engineering Science, 52, 4045–4053.

Iliuta, I., Larachi, F., 1999. The generalized slit model: pressure gradient, liquid holdup and wetting efficiency in gas-liquid trickle flow. Chemical Engineering Science, 54, 5039−5045.

Iliuta, I., Larachi, F., Al-Dahhan, M.H., 2000a. Double-slit model for partially wetted trickle flow hydrodynamics. AIChE Journal, 46, 597−609.

Iliuta, I., Larachi, F., Al-Dahhan, M.H., 2000b. Multiple-zone model for partially wetted trickle flow hydrodynamics. Transactions of the Institution of Chemical Engineers, Part A, 982−990.

Iliuta, I., Larachi, F., 2005. Modeling the hydrodynamics of gas-liquid packed beds via slit models: A review. International Journal of Chemical Reactor Engineering, 3, R4.

Jiang, Y., Khadilkar, M.R., Al-Dahhan, M.H., Duduković, M.P., 1999. Two-phase flow distribution in 2D trickle-bed reactors. Chemical Engineering Science, 54, 2409−2419.

Jiang, Y., Khadilkar, M. R., Al-Dahhan, M. H., Duduković, M. P., 2002. CFD of multiphase flow in packed-bed reactors: I. k-fluid modeling issues. AIChE Journal, 48, 701−715.

Kan, K.M., Greenfield, P.F., 1978. Multiple hydrodynamic states in cocurrent two-phase downflow through packed beds. Industrial and Engineering Chemistry Process Design and Development, 17, 482–485.

Kolomaznık, K., Soukup, J., Prchlık, J., Zapletal, V., Růžička, V., 1974. Experimental determination of the spreading coefficient. Collection of Czechoslovak Chemical Communications, 39, 216–219.

Kundu, A., Nigam, K.D.P., Verma, R.P., 2003. Catalyst wetting characteristics in trickle-bed reactors. AIChE Journal, 49, 2253−2263.

Lakota, A., Levec, J., 1990. Solid-liquid mass transfer in packed-beds with cocurrent downward two-phase flow. AIChE Journal, 36, 1444–1448.

Larachi, F., Laurent, A., Midoux, N., Wild, G., 1991. Experimental study of a trickle-bed reactor at high pressure: Two-phase pressure drop and liquid saturation. Chemical Engineering Science, 46, 1233−1246.

Larachi, F., Belfares, L., and Grandjean, B.P.A., 2001. Prediction of liquid-solid wetting efficiency in trickle flow reactors. International Communications in Heat and Mass Transfer, 28, 595–603.

Laroussi, C., de Backer, L.W., 1979. Relations between geometrical properties of glass beads media and their main $\psi(\theta)$ hysteresis loops. Soil Science Society of America Journal, 43, 646–650.

Lazzaroni, C.L., Keselman, H.R., Figoli, N.S., 1988. Colorimetric evaluation of the efficiency of liquid-solid contacting in trickle flow. Industrial & Engineering Chemistry Research, 27, 1132–1135.

Levec, J., Sáez, A.E., Carbonell, R.G., 1986. The hydrodynamics of trickling flow in packed beds. Part II: Experimental observations. AIChE Journal, 32, 369–380.

Leverett, M.C., 1941. Capillary behaviour in porous solids. Transactions of the AIME, 142, 152–168.

Ligny, C.L., 1970. Coupling between diffusion and convection of the matter by fluid flow through packed beds. Chemical Engineering Science, 25, 1177−1181.

Likos, W.J., Lu, N., 2004. Hysteresis of capillary stress in unsaturated granulated soil. Journal of Engineering Mechanics (ASCE), 130, 646−655.

Lin, S.-Y., Chang, H.-C., Lin, L.-W., Huang, P.-Y., 1996. Measurement of dynamic/advancing/receding contact angle by video-enhanced sessile drop tensiometry. Review of Scientific Instruments, 67, 2852−2858.

Loudon, D., van der Merwe, W., Nicol, W., 2006. Multiple hydrodynamics states in trickle flow: Quantifying the extent of pressure drop, liquid holdup and gas-liquid mass transfer variation. Chemical Engineering Science, 61, 7551–7562.

Lutran, P.G., Ng, K.M., Delikat, E.P., 1991. Liquid distribution in trickle-beds. An experimental study using computer-assisted tomography. Industrial & Engineering Chemistry Research, 30, 1270–1280.

Maier, R.S., Kroll, D.M., Bernard, R.S., Howington, S.E., Peters, J.F., Davis, H.T., 2003. Hydrodynamic dispersion in confined packed beds. Physics of Fluids, 15, 3795–3815.

Marcandelli, C., 1999. *Hydrodynamique, transfert de chaleur particule-fluide et distribution des phases dans les réacteurs à lit fixe à écoulement à co-courant descendant de gaz et de liquide*. Doctoral Thesis. INPL, Nancy, France.

Marchot, P., Crine, M., L'Homme, G., 1992. Rational description of the trickle flow through packed beds. II: Radial spreading of the liquid. Chemical Engineering Journal, 48, 61–70.

Mayer, R.P., Stowe, R.A., 1966. Mercury porosimetry: Filling of tortoidal void volume following breakthrough between packed spheres. Journal of Physical Chemistry, 70, 3867−3873.

Mayer, R.P., Stowe, R.A., 2005. Nodoids and tortoids: Comparison of two geometries for the meniscus profile of a wetting liquid between two touching isolated spheres and extensions to the model of a collection of packed spheres. Journal of Colloid and Interface Science, 285, 781−788.

van der Merwe, W., Maree, C., Nicol, W., 2004. Nature of residual liquid holdup in packed beds of spherical particles. Industrial & Engineering Chemistry Research, 43, 8363−8368.

van der Merwe, W., Nicol, W., 2005. Characterization of multiple flow morphologies within the trickle flow regime. Industrial & Engineering Chemistry Research, 44, 9446–9450.

Mills, P.L., Duduković, M.P., 1981. Evaluating of liquid-solid contacting in trickle-bed reactors by tracer methods. AIChE Journal, 27, 893−904; see errata AIChE Journal, 1982, 28, 526.

Moseley, W.A., Dhir, V.K., 1996. Capillary pressure-saturation relations in porous media including the effect of wettability. Journal of Hydrology, 178, 33−53.

Mueller, G.E., 1991. Prediction of radial porosity distribution in randomly packed fixed beds of uniformly sized spheres in cylindrical containers. Chemical Engineering Science, 46, 706−708.

Murthy, D.S., Sivakumar, S.V., Kant, K., Rao, D.P. 2008. Process intensification in a "simulated moving-bed" heat regenerator. Journal of Heat Transfer, 130, 091801-1–8.

Narasimhan, C.S.I., Verma, R.P., Kundu, A., Nigam, K.D.P., 2002. Modeling hydrodynamics of trickle-bed reactors at high pressure. AIChE Journal, 48, 2459−2474.

Novy, R.A., Toledo, P.G., Davis, H.T., Scriven, L.E., 1989. Capillary dispersion in porous media at low wetting phase saturation. Chemical Engineering Science, 44, 1785−1797.

Oh, W.-S., Shen, C., Alegre, B., Anusavice, K.J., 2002. Wetting characteristic of ceramic to water and adhesive resin. The Journal of Prosthetic Dentistry, 88, 616−621.

Onda, K., Takeuchi, H., Maeda, Y., Takeuchi, N., 1973. Liquid distribution in a packed column. Chemical Engineering Science, 28, 1677−1683.

Pinna, D., Tronconi, E., Tagliabue, L., 2001. High interaction regime Lockhart-Martinelli model for pressure drop in trickle-bed reactors. AIChE Journal, 47, 19–30.

Pironti, F., Mizrahi, D., Acosta, A., González-Mendizabal, D., 1999. Liquid-solid wetting factor in trickle-bed reactors: its determination by a physical method. Chemical Engineering Science, 54, 3793–3800.

Porter, K.E., 1968. Liquid flow in packed columns. Part I: The rivulet model. Transactions of the Institution of Chemical Engineers, 46, T69−T73.

Porter, K.E., Barnett, V.D., Templeman, J.J., 1968. Liquid flow in packed columns. Part II: The spread of liquid over random packings. Transactions of the Institution of Chemical Engineers, 46, T74−T85.

Porter, K.E., Templeman, J.J., 1968. Liquid flow in packed columns. Part III: Wall flow. Transactions of the Institution of Chemical Engineers, 46, T74−T85.

Potucek, F., 1997. Washing of pulp fibre bed. Collection of Czechoslovak Chemical Communications, 62, 626−644.

Prchlík, J., Soukup, J., Zapletal, V., Růžička, V., 1975. Liquid distribution in reactors with randomly packed porous beds. Collection of Czechoslovak Chemical Communications, 40, 845−855.

Rao, V.G., Ananth, M.S., Varma, Y.B.G., 1983. Hydrodynamics of two-phase cocurrent downflow through packed beds. AIChE Journal, 29, 467–483.

Ratnam, G.S.V., Ananth, M.S., Varma, Y.B.G., 1983. A model for the pressure drop in gas-liquid cocurrent downflow through packed beds. Chemical Engineering Journal, 51, 19–28.

Ravindra, P.V., Rao, D.P., Rao, M.S., 1997. Liquid flow texture in trickle- bed reactors: An experimental study. Industrial & Engineering Chemistry Research, 36, 5133−5145.

Ring, Z.E., Missen, R.W., 1989. Trickle-bed reactors: an experimental study of partial wetting efficiency. AIChE Journal, 35, 1821–1828.

Ring, Z.E., Missen, R.W., 1991. Trickle-bed reactors: Tracer study of liquid holdup and wetting efficiency at high temperature and pressure. Canadian Journal of Chemical Engineering, 69, 1016−1020.

Rose, W., 1958. Volumes and surface areas of pendular rings. Journal of Applied Physics, 29, 987−691.

Sáez, A.E., Carbonell, R.G., 1985. Hydrodynamic parameters for gas–liquid cocurrent flow in packed beds. AIChE Journal, 31, 52−62.

Sai, P.S.T., Varma, Y.B.G., 1987. Pressure drop in gas-liquid downflow through packed beds. AIChE Journal, 33, 2027–2036.

Sai, P.S.T., Varma, Y.B.G., 1988. Flow pattern of the phases and liquid saturation in gas-liquid cocurrent downflow through packed beds. Canadian Journal of Chemical Engineering, 66, 353–360.

Sahimi, M., Hughes, B.D., Scriven, L.E., Davis, H.T., 1986a. Dispersion in flow through porous media − I. One-phase flow. Chemical Engineering Science, 41, 2103−2122.

Sahimi, M., Heiba, A.A., Davis, H.T., Scriven, L.E., 1986b. Dispersion in flow through porous media − II. Two-phase flow. Chemical Engineering Science, 41, 2123−2136.

Saroha, A.K., Nigam, K.D.P., Saxena, A.K., Kapoor, V.K., 1998. Liquid distribution in trickle-bed reactors. AIChE Journal, 44, 2044−2052.

Schnitzlein, K., 2001. Modeling radial dispersion in terms of the local structure of packed beds. Chemical Engineering Science, 56, 579−585.

Scott, A.H., 1935. Liquid distribution in packed towers. Chemical Engineering Research & Design, 13a, 211–217.

Sederman, A.J., Gladden, L.F., 2001. Magnetic resonance imaging as a quantitative probe of gas–liquid distribution and wetting efficiency in trickle-bed reactors. Chemical Engineering Science, 56, 2615–2628.

Specchia, V., Baldi, G., 1977. Pressure drop and liquid holdup for two phase concurrent flow in packed beds. Chemical Engineering Science, 32, 515–523.

Specchia, V., Baldi, G., Gianetto, A., 1978. Solid-liquid mass transfer in concurrent two-phase flow through packed beds. Industrial and Engineering Chemistry Process Design and Development, 17, 362–367.

Sun, C.G., Yin, F.H., Afacan, A., Nandakumar, K., Chuang, K.T., 2000. Modelling and simulation of flow maldistribution in random packed columns with gas-liquid countercurrent flow. Chemical Engineering Research and Design, 78, 378–388.

Tosun, G., 1984. A study of cocurrent downflow of nonfoaming gas-liquid systems in a packed bed. 2. Pressure drop: search for a correlation. Industrial and Engineering Chemistry Process Design and Development, 23, 35–39.

Tung, V.X., Dhir, V.K., 1988. A hydrodynamic model for two-phase flow through porous media. International Journal of Multiphase Flow, 14, 47−65.

Urseanu, M.I., Boelhouwer, J.G., Bosman, H.J.M., Schroijen, J.C., Kwant, G., 2005. Estimation of trickle-to-pulse flow regime transition and pressure drop in high-pressure trickle bed reactors with organic liquids. Chemical Engineering Journal, 111, 5–11.

Wammes, W.J.A., Middelkamp, J., Huisman, W.J., deBaas, C.M., Westerterp, K.R., 1991. Hydrodynamics in a cocurrent gas-liquid trickle bed at elevated pressures, AIChE Journal. 37, 1849−1862.

Wammes, W.J.A., Westerterp, K.R., 1991. Hydrodynamics in a pressurized cocurrent gas-liquid trickle-bed reactor. Chemical Engineering & Technology, 14, 406−413.

Westerterp, K.R., Wammes, W.J.A., 2005. *Three-phase trickle-bed reactors*. In Ullmann's Encyclopedia of Industrial Chemistry. Viley-VCH Verlag GmbH & Co. KGaA, Weinheim.

Xiao, Q., Anter, A.M., Cheng, Z.M., Yuan, W.K., 2000. Correlations for dynamic liquid holdup under pulsing flow in a trickle-bed reactor. Chemical Engineering Journal, 78, 125–129.

Yang, D., Udey, N., Spanos, T.J.T., 1998. Automaton simulations of dispersion in porous media. Transport in Porous Media, 32, 187–198.

Yin, F.H., Afacan, A., Nandakumar, K., Chuang, K.T., 2002. CFD simulation and experimental study of liquid dispersion in randomly packed metal pall rings. Transactions of the Institution of Chemical Engineers Part A, 80, 135−144.